Numerical analysis of high-speed railway slab tracks using calibrated and validated 3D time-domain modelling

A. F. Esen[1,2] · O. Laghrouche[2] · P. K. Woodward[1] · D. Medina-Pineda[3] · Q. Corbisez[3] · J. Y. Shih[4] · D. P. Connolly[1]

Abstract

Concrete slabs are widely used in modern railways to increase the inherent resilient quality of the tracks, provide safe and smooth rides, and reduce the maintenance frequency. In this paper, the elastic performance of a novel slab trackform for high-speed railways is investigated using three-dimensional finite element modelling in Abaqus. It is then compared to the performance of a ballasted track. First, slab and ballasted track models are developed to replicate the full-scale testing of track sections. Once the models are calibrated with the experimental results, the novel slab model is developed and compared against the calibrated slab track results. The slab and ballasted track models are then extended to create linear dynamic models, considering the track geodynamics, and simulating train passages at various speeds, for which the Ledsgård documented case was used to validate the models. Trains travelling at low and high speeds are analysed to investigate the track deflections and the wave propagation in the soil, considering the issues associated with critical speeds. Various train loading methods are discussed, and the most practical approach is retained and described. Moreover, correlations are made between the geotechnical parameters of modern high-speed rail and conventional standards. It is found that considering the same ground condition, the slab track deflections are considerably smaller than those of the ballasted track at high speeds, while they show similar behaviour at low speeds.

Keywords High-speed railways · Slab track · New ballastless track · Ballasted track · Critical speeds · Finite element modelling · Calibration of numerical models

1 Introduction

In the past two decades, high-speed rail infrastructure developed at a very rapid pace. The construction of the HS2 line has been approved in the UK and thousands of kilometres are being built worldwide, especially in China. However, the increase in train speeds has led to new issues with the train–track–soil dynamic behaviour being one of them. Therefore, many authors have investigated the effect on the

ground and on neighbouring structures caused by the passage of high-speed trains running at speeds close to critical velocities. This situation occurs on soft soils when the train speed approaches the ground Rayleigh velocity, leading to the development of a Ground Mach cone and to significant levels of transmitted ground vibrations [1]. In such situations, the transient track displacement can be as high as 5 times the corresponding static deflection, which obviously poses a threat of train derailment and leads to an accelerated degradation of the track infrastructure. This potentially affects the surrounding environment, causing malfunctioning of sensitive equipment, nuisance to inhabitants and even initiate cracks in structures. The demand for high and ultra-high speeds, higher traffic intensity, increased vibration levels and critical velocity cases, lower life-cycle costs, energy consumption and emission, and global warming associated issues led to the development of a new railway track system: the slab track. Slab tracks, also known as non-ballasted or ballastless tracks, consist of concrete or asphalt layer replacing the ballast. This kind of structure provides higher

✉ A. F. Esen
ae2023@hw.ac.uk

1 Institute for High-Speed Rail and System Integration, University of Leeds, Leeds LS2 9JT, UK

2 Institute for Infrastructure and Environment, Heriot-Watt University, Edinburgh EH14 4AS, UK

3 Alstom Transport, Saint-Ouen, France

4 Birmingham Centre for Railway Research and Education, University of Birmingham, Birmingham B15 2TT, UK

stability, durability, even ride quality, and low requirements for maintenance [2–10].

Concrete slab tracks are classified as discrete rail support and continuous rail support tracks. In the discrete rail support systems, the rail is attached to the track with separate supporting points, whereas in the continuous rail support systems, the rail is supported by a continuous elastic compound such as cork and polyurethane. A new high-performance ballastless trackform has been developed by Alstom, in France, based on the experience of concrete track behaviour and including considerations of automated installation techniques [8]. The cast-in slab track *so-called* new ballastless track (NBT) is designed for high installation speeds using the mechanised track-laying technology called *Appitrack* (Fig. 1a)[8]**.**

Some of the most common slab tracks used all over the world mentioned in Refs. [4, 5, 9] are listed as follows:

- Sleepers or blocks encased in in situ concrete: Rheda (German), Zublin (German)
- In situ concrete without sleepers: NBT (French)

- Precast concrete slab segments: Max-Bögl (German), ÖBB Porr (Austrian), Shinkansen (Japan)
- Continuously embedded rail: Edilon (Dutch), BBEST Balfour Beatty (British)

Figure 1b shows a Max-Bögl slab track, which is a prefabricated and prestressed reinforced concrete track. The prefabricated slabs are delivered to a field and positioned 4 mm above the cast-in concrete layer and are coupled via a cementitious mortar poured in between. A section of a Max-Bögl slab track is used as part of the experimental investigation linked to the current research [11, 12].

The literature shows a large number of studies investigating the performance of the slab track infrastructure, including semi-analytical, experimental and numerical investigations. For the latter, numerous numerical models have been developed to study the track performance and ground-transmitted vibrations. Multi-dimensional track–soil models and single-degree or multi-degrees of freedom vehicle models have been used to assess the performance of the track at various train speeds and soil parameters, including critical speeds issues.
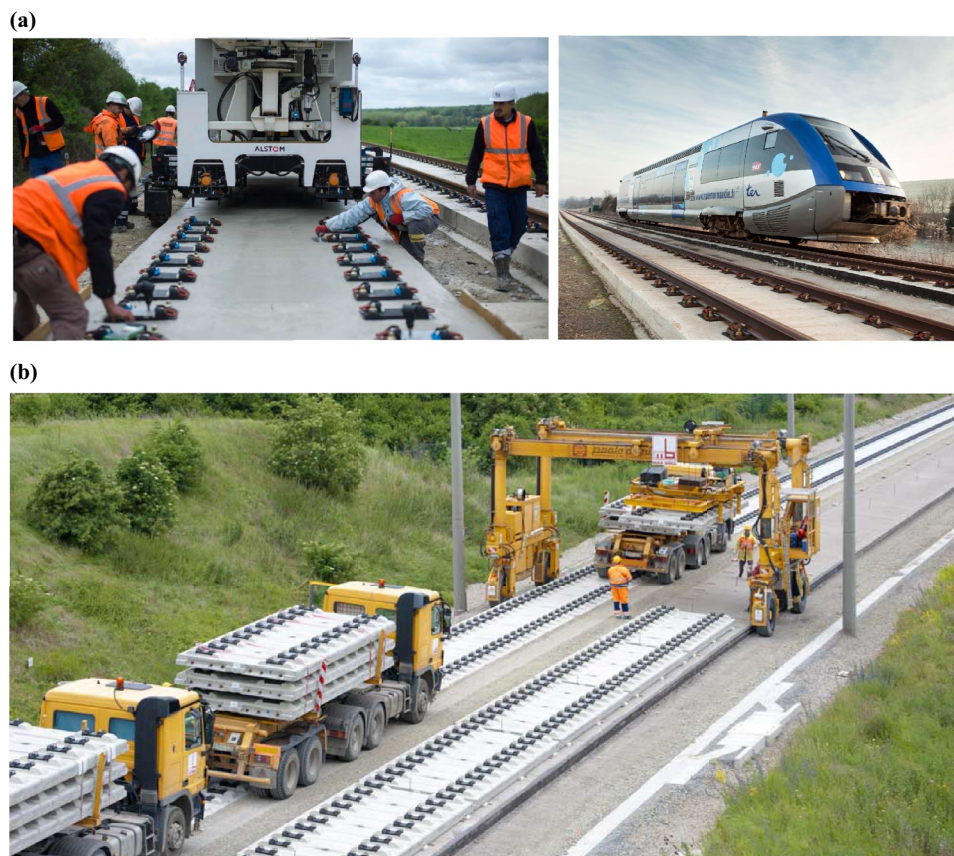
Fig. 1 Reinforced concrete slab tracks: **a** cast in-situ slab track NBT (courtesy of Alstom); **b** precast slab track Max-Bögl (courtesy of Max-Bögl)

1.1 Critical velocity issues

Trains traversing soft soils are known to reach a critical situation where their speed may approach or even exceed the ground wave velocities, resulting in critical track velocity issues. This is accompanied by elevated transient displacements leading to possible track uplift and increased subgrade deterioration [13–15].

One of the most famous critical velocity documented case is the Ledsgård example, in Sweden, where large vibrations were observed on the X-2000 service between Gothenburg and Malmo [16–20]. The X-2000 train, which was formed of a locomotive and 4 passenger carriages, performed test runs at speeds varying between 10 and 200 km/h. The soil underneath the track mainly consisted of dry crust, organic clay and marine clay. Its geotechnical parameters were known up to 50 m depth. To solve this issue, the mitigation strategy required 13 m deep lime/cement stabilisation columns underneath the ballasted track for about 1.5 km, which was achieved at considerable expense. Moreover, the line was taken totally out of commission during the renewal.

1.2 Track models

Track structures are modelled numerically to simulate the dynamic interaction of their components. The choice of the model is a crucial step to fully investigate the track behaviour. The model can consist of one-layer or multi-layers and can have a continuous or discrete support mechanism.

Models of 2D, 3D or 2.5D subgrade underneath the track can be used according to the focus of the problem [20, 21].

Euler-Bernoulli beam (E-B beam) theory and Rayleigh-Timoshenko beam (R-T beam) theory, which consider the rail as it is one of the primary components of railway track, are used to investigate the rail bending (R-T beam also considers shear deformation) with analytical models [22]. 2D models are used to investigate the vertical track performance, which are based on the widely used formulation called beam on elastic foundation (BOEF). The vast majority of railway track models have evolved from the Euler–Bernoulli beam placed over a spring–dashpot–mass model [17, 23] or based on finite element (FE) models created using commercial software [24]. However, 2D models are not fully capable of simulating the ground-borne vibration and wave propagation. Moreover, due to the availability of fast computers, 2.5D and 3D models have been developed to investigate the behaviour of railway tracks under moving wheel loads. For example, 2.5D models are created via 3D models which are divided into thin element slices. This method is followed to reduce the computational requirements while obtaining approximate 3D solutions. Such 2.5D FEM models were created to investigate ground vibrations generated by high-speed train passages by various researchers [25–29]. A 2.5D time–frequency model was created in Ref. [30] to study the railway vibrations due to rail-wheel defects. Other researchers [31–33] combined the thin-layer method (TLM) with the 2.5D finite element modelling to predict the ground vibrations induced by passing trains at various speeds.

Ground induced vibration due to the passage of a high-speed locomotive was investigated using a coupled
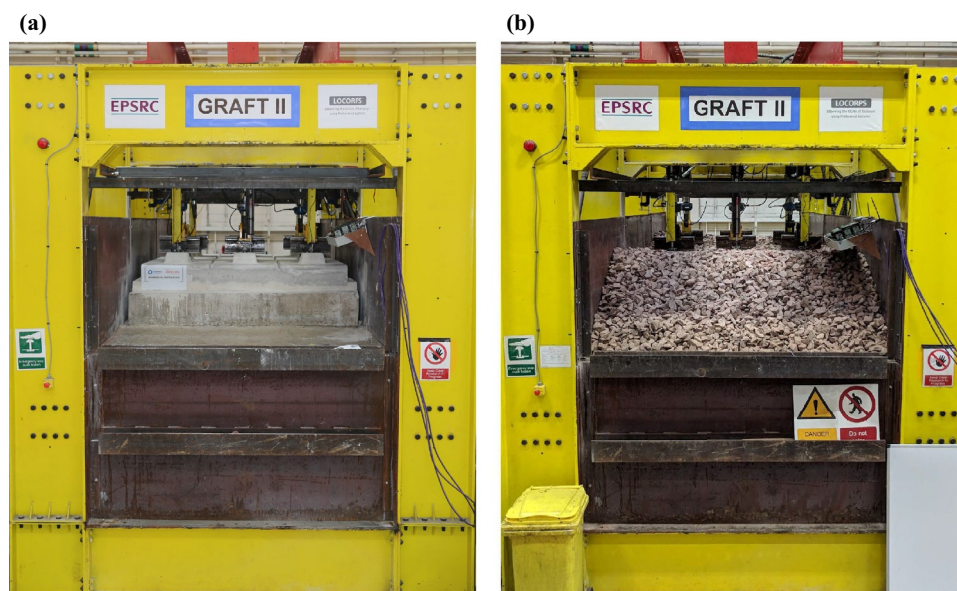
Fig. 2 Full-scale testing of **a** the slab track and **b** the ballasted track
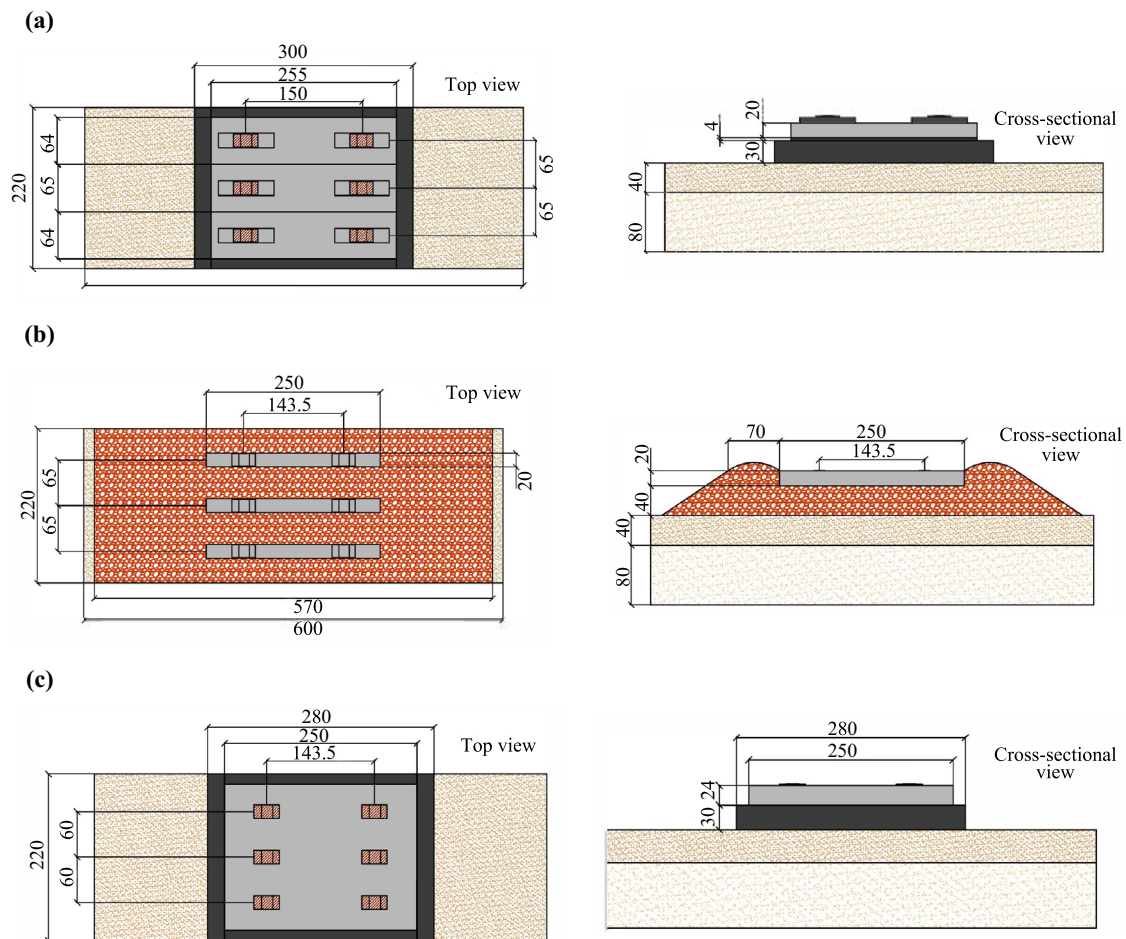
Fig. 3 The dimensions of **a** Max-Bögl slab track, **b** the ballasted track and **c** NBT (unit: cm)

train–track dynamic finite element model using 3D ground modelling [1, 34]. A full 3D model with a similar coupling approach was developed by Banimahd et al. 35] using an in-house software called DART3D (Dynamic Analysis of Railway Track 3D) to investigate deflection changes in the vicinity of transition zones. Woodward et al. [14] used DART3D to study ground dynamics when a train approaches the critical track velocity. Further 3D models based on the Ledsgård case were developed by using Abaqus [19, 36, 37] and Midas-GTS [38]. A 3D model utilising infinite elements and implementing absorbing boundary conditions of Lysmer and Kuhlemeyer [39] was developed by Connolly et al. [40, 41] and was validated using field recordings of the high-speed line Paris-Brussels and the mixed passenger and freight line Edinburgh–London, respectively. Gao et al. [42, 43] also studied the critical velocity issue of soft soils using a 3D dynamic model and validated it by using a field investigation carried out on Amtrak's Northeast Corridor in the USA. Theyssen et al. [44] calibrated and validated 3D slab track models using acceleration data collected from a full-scale testing rig. The rig was used to test various slab tracks

constructed according to Chinese high-speed railway standards [45]. Further FE dynamic modelling of slab tracks was performed to study train–slab track interaction in ANSYS [46] and Abaqus [47]. Comprehensive FE models on ground bourne vibrations caused by high-speed train passage were investigated in China [48, 49].

1.3 Vehicle models and moving loads

Various numerical models have been developed to describe moving loads due to passing trains. Fryba [50] used analytical expressions to model a moving point load positioned on an elastic half space in order to simulate track dynamics at critical velocity. Krylov [51] and Dieterman and Metrikine [52] later used a moving load to represent train–wheel theoretical expressions for the track structure and Green's functions for the soil. A rail was formed of beam elements with nodes, which Hall [19] referred to as loading nodes. A point load, which was distributed as triangular pulses on three nodes, moved from one node to another. Dong et al. [33] also implemented a moving point load where each wheel

had a downward force, and all the forces were combined using the superposition method to form a 5-car long X2000 train model travelling across the Ledsgård mentioned track. The model assumed that the horizontal surface is infinite on which the moving loads were running at a prescribed speed.

Galvín et al. [34] used a multi-body model for an axle with primary and secondary suspensions in a fully three-dimensional coupled finite-element–boundary-element (FE–BE) model simulating high-speed train–track–soil–structure dynamic interaction in the time domain. Kouroussis et al. [53] modelled a multi-body vehicle formed of a car with a bogie and two axles. The vertical force exerted on the rail was based on the Hertzian stiffness and took account of the rail defect. In this study, a special method was used to account for the vehicle–track and track–ground analyses separately, assuming a much higher soil stiffness than the ballast stiffness. In Abaqus, infinite elements were used to model wave radiation to infinity, and were combined with a finite element model of the soil and the multi-body model of the vehicle [53]. Connolly et al. [40] used a similar approach and modelled a Thalys train travelling in France, Germany, and Belgium, but added a FORTRAN-defined moving load subroutine to the Abaqus model. The explicit model employed VDLOAD and VUFIELD subroutines to simulate half of the vehicle. The non-Hertzian contact condition between the wheel and rail was used for the coupling. The interaction of the vehicle–track and ground was simulated in the time domain and validated using field data from a high-speed line. El Kacimi et al. [1] created a quarter train model coupled to a 3D FE model in which the wheel–rail contact was based on nonlinear Hertzian conditions.

A moving load method based on vehicle–bridge interaction (VBI) in a high-speed railway bridge analysis was developed by Yang and Yau [54]. The train was represented as a series of sprung masses lumped at the bogie positions and the bridge with track irregularities was modelled using beam components. This moving spring–mass numerical approach has been implemented in Abaqus by Saleeb and Kumar [55] and Shih et al. [56]. An oscillator moving on a simply supported elastic beam was modelled in the time domain using the finite sliding contact model in Abaqus. The default contact property "*hard contact*" was used to simulate the sliding motion on a frictionless surface using the node-to-surface contact function. The displacement of the moving object along the direction of travel at each time phase was used to achieve a constant moving speed. This method reduces the simulation CPU times of a moving load compared to the user-subroutine defined moving loads. This method was used for a multi-car X2000 train by Shih et al. [53] and Sun [37] to develop 3D models of the Ledsgård track case. In this research, a similar method developed by Shih et al. [36] is implemented for the sake of computational efficiency and results accuracy.
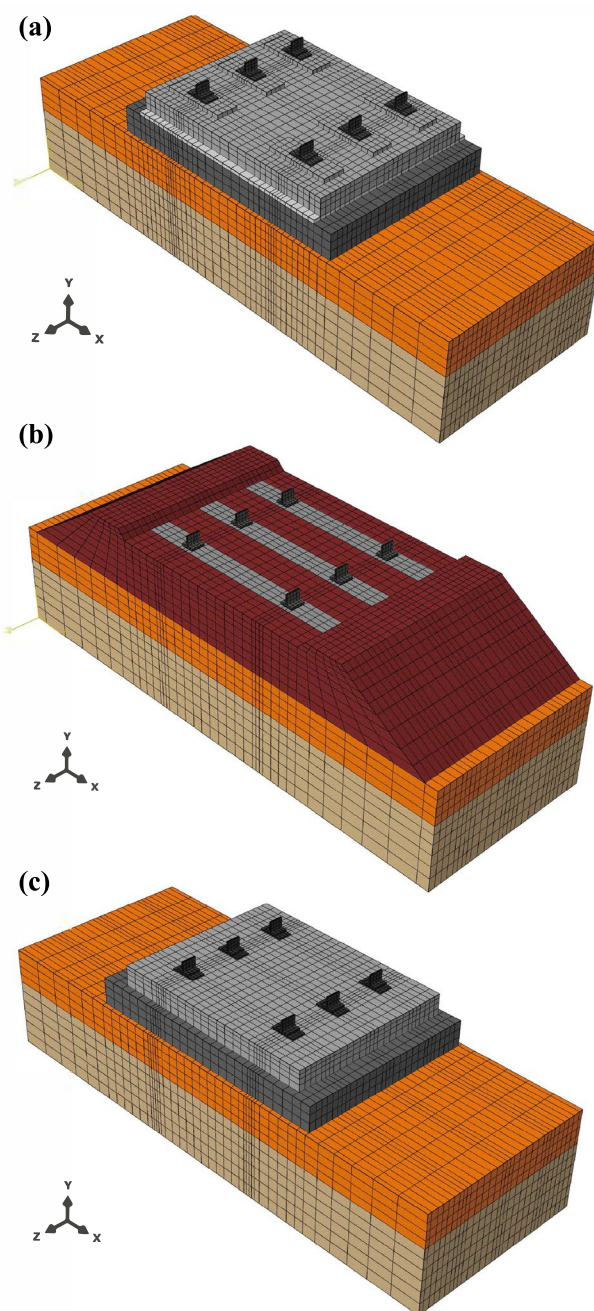
Fig. 4 3D models: **a** Max-Bögl slab track; **b** ballasted track; **c** NBT slab track

This paper is organised as follows. After the current introduction, Sect. 2 presents the methodology followed in this research work. Section 3 describes the stages of the numerical model development. The 3D model of the experimental setup and the calibration steps using the full-scale testing results to identify the material properties of the track subgrade are presented. The calibration process is discussed in detail. Section 3 ends with an extended 3D model simulating

a train passage over a track–soil model to assess the performance of NBT under critical velocity conditions. The details of the track–soil domain, vehicle models and moving loads are also provided. Section 4 discusses the NBT results against those of a ballasted track model based on the in situ data obtained in Ledsgård, Sweden. The final section summarises the outcomes of this research work and presents the main concluding remarks.

2 Methodology

In this study, linear elastic three-dimensional (3D) finite element (FE) models of the ballasted and slab tracks are developed to investigate the transient behaviour of the tracks. The followed approach is described as follows:

1. First, in a full-scale laboratory investigation, a ballasted section and a slab track section were built in the Geopavement and Railway Accelerated Fatigue Testing (GRAFT-II) facility [11, 12, 57]. The tracks were positioned on an embankment which was constructed according to high-speed railway standards. The forces applied on the tracks and the resulting displacements of the sleepers/slab and rails were obtained

2. The tracks built in the GRAFT-II facility are modelled in Abaqus. The material parameters of the tracks, which were obtained through laboratory characterisation such as density, Poisson's ratio, and Young's modulus, are
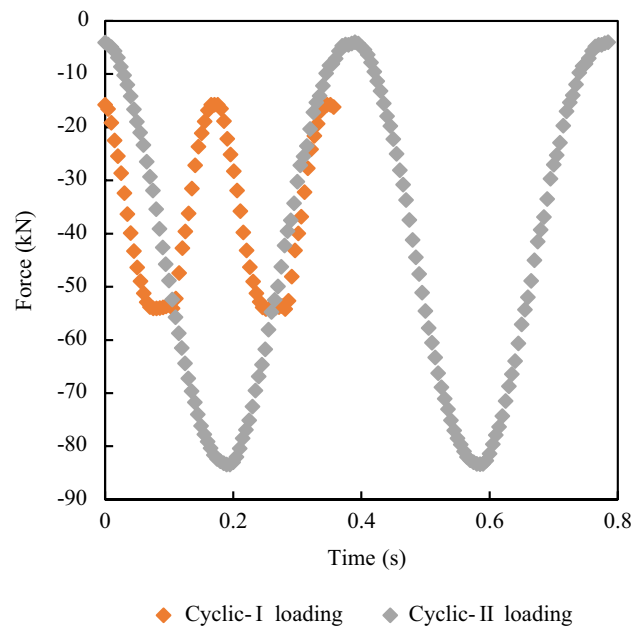

Fig. 5 The cyclic loading applied on each rail during Cyclic-I and II

used in the numerical models. The same loading combinations and time increments were used in the numerical model analyses. The displacement transducers positioned on the rails, the sleepers and the slab were used to compare the displacements of the corresponding nodes in the FE models

Table 1 Parameters of Max-Bögl slab track obtained from the theoretical and numerical analysis

Tracks	Track components	Density (kg/m³)	Poisson's ration	Young's modulus (MPa)		Info.
				Theoretical	Numerical	
Common for all tracks	Rail	7850	0.3	210,000	210,000	60E1
	EVA	1000	0.3	450	450	1200 kN/mm (Static) 1800 kN/mm (Dynamic)
	Steel plate	7850	0.3	210,000	210,000	210 GPa
	EPDM	1200	0.4	10	10	22.5 kN/mm (Static) 40 kN/mm (Dynamic)
	FPL	2144	0.35	270–440	500	133.55 Mpa (E_{V2} PLT test)
	Subgrade	2091	0.35	130–225	250	67.71 Mpa (E_{V2} PLT test)
Max-Bögl	Slab	2500	0.25	38,000	38,000	38 GPa
	Grout	2000	0.25	25,000	25,000	25 GPa
	HBL	2400	0.25	18,000	18,000	18 GPa
Ballasted track	Sleeper	2500	0.15	38,000	38.000	G44
	Ballast	2000	0.30	110	110	UIC719Rb
NBT	Slab	2500	0.25	38,000	38,000	38 GPa
	HBL	2400	0.25	18,000	18,000	18 GPa

In the rightmost 'Info' column, 60E1, also known as UIC60, is a rail model manufactured according to the European standard EN 13674–1; data with 'Static' and 'Dynamic' represent the static and dynamic stiffness of the pads, respectively; E_{V2} PLT test in parentheses stand for the E_{V2} values obtained through plate loading tests; data with units of GPa are Young's modulus of the materials; G44 and UIC719Rb are traditional UK sleeper and EU ballast types, respectively
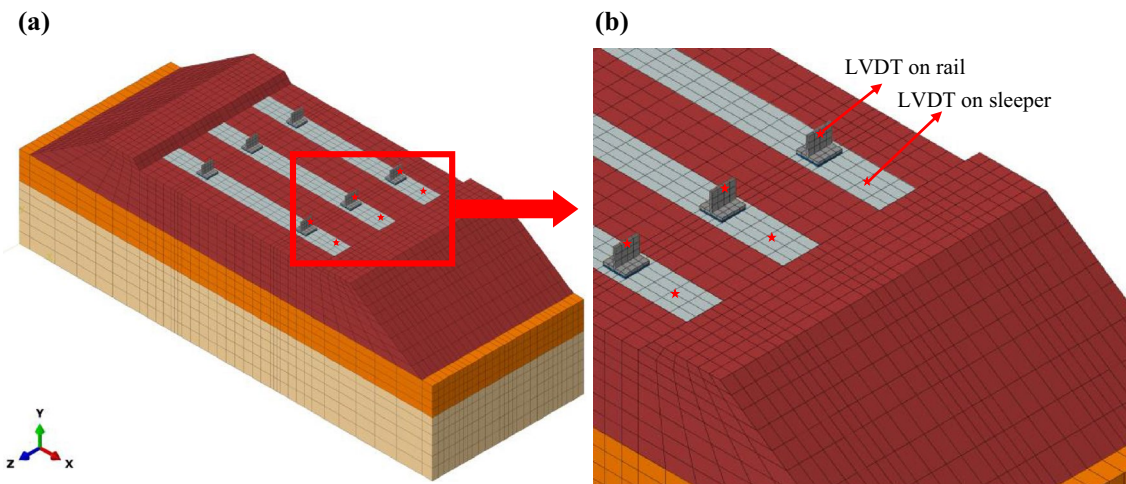
Fig. 6 The location of the nodes for displacement output: **a** the LVDTs on the rails and sleepers; **b** close up view

3. The experimental testing results are used to compare the short-term behaviour of the tracks. The geotechnical and geometrical model parameters of the 3D models are then calibrated

4. The calibrated track and soil parameters are then used with the NBT slab track model for which the results are compared against the Max-Bögl slab track results

5. The calibration stage is then followed by the full dynamic model analysis of the NBT model. The subgrade model is extended in the transversal, longitudinal and in-depth directions to include the 3D soil medium and simulate train passages at various speeds

6. The developed models are validated using results available in the literature including critical velocity cases, which themselves were validated against field measurements recorded in Ledsgård, Sweden [16, 17]. The finite sliding contact in Abaqus is used to model a moving oscillator to replicate the moving dynamic train loading. The node-to-surface contact function is used to simulate a sliding motion on a frictionless surface using the default contact property "hard contact" without contact damping

7. Various train speeds are investigated to identify the critical velocity effect in the NBT and ballasted track cases.

3 Numerical model development

The stages of the full 3D FE model creation are described in detail in this section.

3.1 Full-scale laboratory testing

Full-scale testing was carried out on three-sleeper sections of ballasted and slab tracks by simulating moving loads at 360 km/h in the GRAFT-II facility. The testing rig is 2.2 m wide, 6 m long and 3.8 m high, which is supported by a thick composite base. The tracks are supported by a low-level fully confined conventional embankment. First, a three-sleeper section of a precast concrete Max-Bögl slab track was tested under controlled laboratory conditions, followed by a ballasted track (Fig. 2). Both superstructures were supported by a 1.2 m deep subgrade and frost protection layer, in accordance with high-speed railway design standards. Two different axle load magnitudes were applied statically, and then cyclically/dynamically, using 6 actuators to replicate moving train axle loads. The overall aim was to assess the performance of the tracks, in terms of transient displacements and total settlements, as well as stress levels at different locations of the substructures [11, 57].

The sections of the slab track and ballasted track resting on the conventional embankment were modelled in Abaqus. It is worth recalling that the substructure was composed of a well-compacted 0–6 mm graded sand mixture. The optimum moisture content, which was 5%, was determined by standard and modified proctor compaction tests, which were carried out following the procedures stated in BS 1377-4:1990 [58]. The structural characteristics of unbound materials in railway substructures were determined using the TRRL DCP (A2465) (here TRRL stands for Transport and Road Research Laboratory, Workingham, Berkshire, UK; and DCP stands for dynamic cone penetrometer). DCP readings were taken in the GRAFT-II facility at six different locations, after each compaction stage of the soil. A correlation between the DCP readings and California bearing ratio (CBR) was achieved using the expression $\log 10(CBR) = 2.48 - 1.057 \times \log 10$ (mm/blow) proposed in Ref. [59]. The deflection modulus E_{V2}

(a)

(b)
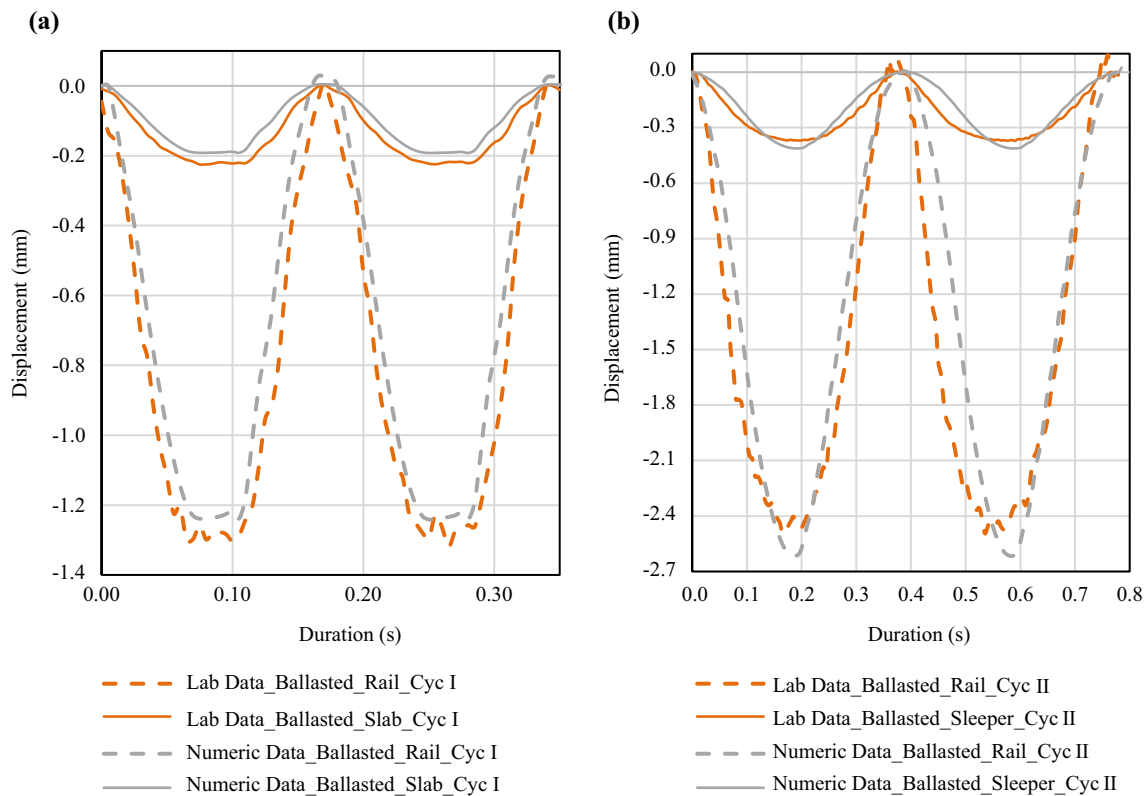
Fig. 7 Comparison of experimental and numerical results of vertical displacements of rails and sleepers of ballasted track under **a** Cyclic-I loading and **b** Cyclic-II loading

was verified using a static plate load test in accordance with DIN-18134 standard [60]. In this work, the E_{V2} value of frost protection layer (FPL) was estimated through the plate load test to be 133.55 MN/m^2 and the E_{V2} value of the subgrade 67.71 MN/m^2. The Young's modulus of the compacted sand was calculated based on the DCP and plate loading test (PLT) results using $E_{dyn} = 2E_{V2} = 100\text{CBR}(\%)$ used in Ref. [4]. Ramos et al. [61] suggested $E_{dyn} = 3.3E_{V2}$ after a calibration process.

The first type of superstructure to be tested was the Max-Bögl slab track. The dimensions of the track are indicated in Fig. 3. The layers from top to bottom were the precast concrete slab track, grout, hydraulically bonded layer (HBL), FPL, and subgrade.

The second tested superstructure was the ballasted track. The used sleepers were the traditional reinforced concrete sleepers named G44 by Tarmac. The ballast thickness right under the sleeper was 40 cm and the total base width of the ballast on the FPL was 570 cm. The track gauge was 150 cm. However, the sleeper spacing was kept the same as that of the slab track sections.

The dimensions of the NBT are given in Fig. 3c. The main difference between NBT and Max-Bögl track is the production methods which are cast-in and prefabricated,

respectively. The width of HBL of NBT is 20 cm smaller than the HBL of the Max-Bögl track and the NBT slab itself is 5 cm less wide than the Max-Bögl slab. Despite the fact that similar fastening system and railpads were employed, the support conditions of the pads and the installation methods are different in each track. The NBT slab is directly cast-in on HBL without any need for a bonding layer like the grout. The rail pads are installed on a fastening system, not directly on the concrete, so there is an intermediate layer made of steel or composite on top of the slab on the NBT, and in the Max-Bögl case, the slab track has a 5 cm thick concrete pad support, which is part of the slab.

A finite element model of the track section tested in the full-scale testing rig was developed using the commercial software Abaqus. The slab and the ballasted tracks on the conventional embankmnet were simulated, with the slab track being a precast reinforced concrete Max-Bögl slab and the ballasted track composed of a ballast layer and precast reinforced concrete sleepers. After performing a mesh size sensitivity study, the calibrated models and chosen parameters were then used to develop the NBT model to investigate its performance in a high-speed rail context, in the dynamic anlaysis part of this work.

(a)

(b)
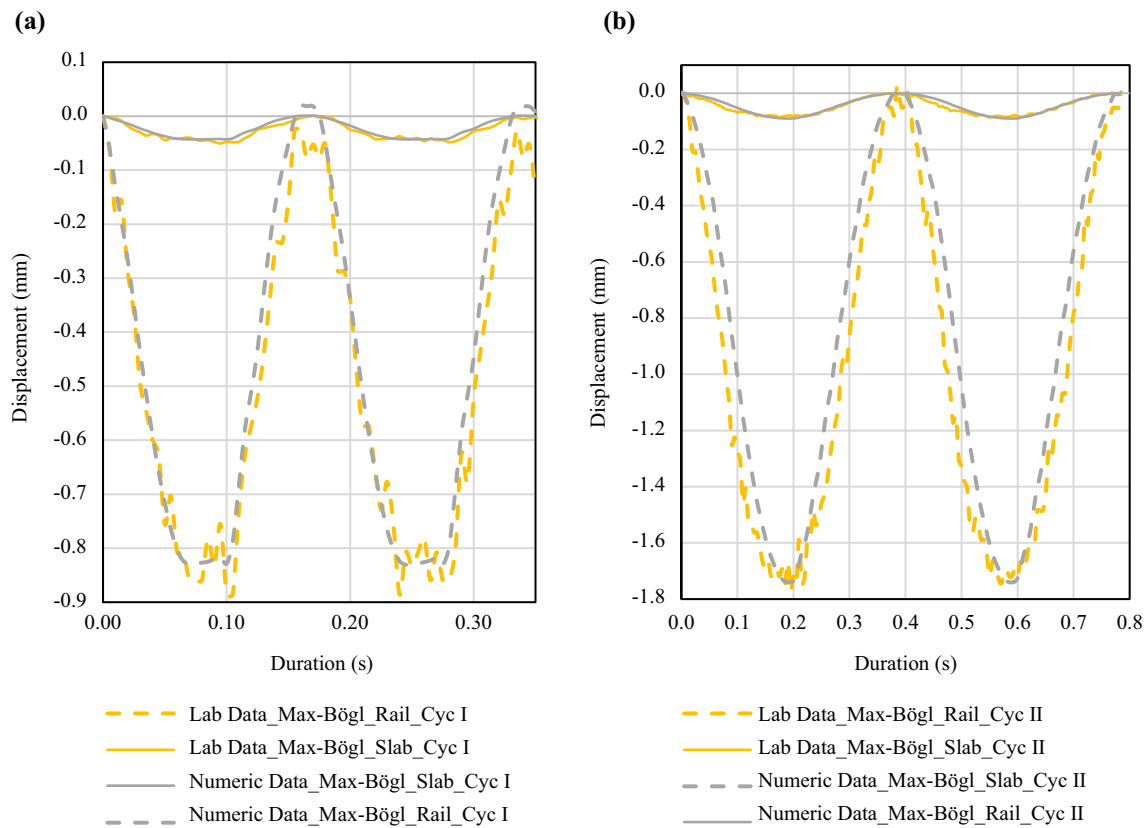
Fig. 8 Comparison of experimental and numerical results of vertical displacements of rails and sleepers of Max-Bögl slab track under **a** Cyclic-I loading and **b** Cyclic-II loading

It is worth mentioning that the experimental results obtained in this research have also served in similar numerical calibrations. Ramos et al. [61] calibrated 3D FE models developed in ANSYS and consisting of slab and ballasted tracks using the experimental results of the GRAFT-II tests. They investigated transient displacement and stress behaviour of the subgrade, and looked at the long-term settlement models based on the experimental and numerical outputs. In another work, Sains-Aja et al. [62] created a 3D FE slab track model also using the commercial software ANSYS and calibrated it via the GRAFT-II laboratory results. They also performed experiments to identify the mechanical characteristics of EVA (ethylene vinyl acetate) and EPDM (ethylene-propylene diene monomer) railpads. Thölken et al. [63] used the GRAFT-II data to calibrate a 3D FE model developed in Abaqus to reproduce the measured displacement and acceleration test results. A parametric analysis was then performed to establish which material characteristics of the system the model was more sensitive to.

3.2 3D modelling of laboratory setup

The 3D FE models created in Abaqus are indicated in Fig. 4. The models were intended to simulate the elastic displacement of the tracks. The used elements were 20-node quadratic solid elements, namely C3D20R. Fine mesh size elements were used immediately under the loads and the coarser elements are used away from the loads. Since the purpose of the rails was to communicate the loads to the layers below, discontinuous rail segments were placed on the tracks, in the experimental testing. However, the rail dimensions were not taken into account. Encastre boundary conditions were implemented on the lateral sides and the bottom face of the soil medium model, so the nodes are fixed to prevent any kind of translation or rotation. This was to simulate the GRAFT-II box walls and base, which were made of rigid metal plates supported by steel I-profile beans, preventing any movements. The materials were assumed to be linear and elastic. This assumption was based on the stress–strain linear relationship employed during the static tests.

Various mesh refinement studies were performed to find the best compromise between computational cost and accuracy. The initial control model was composed of approximately 95,000 nodes. The element sizes were increased in the lateral dimension (*x*-axis in Fig. 4). The mesh size varied between 3.75 and 20 cm for the slab and HBL. They were divided into 3 layers of which the mesh size increased with 1.1 bias ratio along with the depth. The FPL and subgrade had same mesh sizes

(a)

(b)
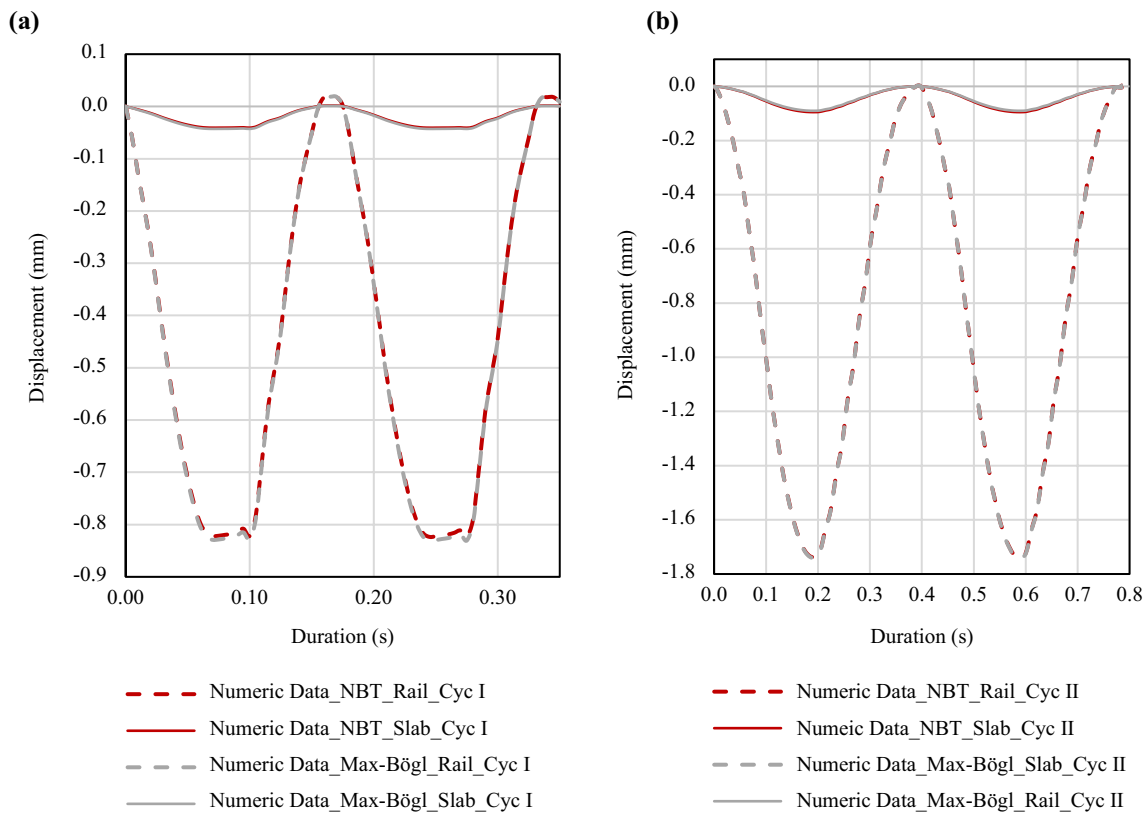
Fig. 9 Numerical comparison of vertical displacement of rails and sleepers of Max-Bögl and NBT slab tracks under **a** Cyclic-I loading and **b** Cyclic-II loading

Table 2 The soil parameters obtained from the experimental and numerical analysis

Soil layers	CBR (%)	E based on CBR (MPa)	E_{V2} of PLT (MPa)	Calculated E (MPa)			
				Lichtberger [4]	Sainz-Aja et al. [62]	Ramos et al. [61]	Current study
FPL	43–120	430–1200	133.1	266.2	500	439.2	500
Subgrade	32–90	320–900	67.7	135.4	500	223.4	250

right under HBL, whereas the mesh size of the soil increased with 1.2 bias ratio further from the track. Similar meshing approach was implemented in ballasted track and NBT. This method reduced the simulation time, as the displacements and stresses further away from the track were negligibly small.

The models consisted of two layers namely substructure and superstructure. The layers were attached using the tie constraint method of Abaqus. A tie constraint connects two surfaces to prevent relative motion between them. It limits translational degrees of freedom but not rotational ones. During the model development, a unified solid element was employed, with varying material parameters assigned to distinguish between components such as HBL and slab. While other layers were created using a similar method, where the whole layer was a single solid element

with varying material properties to distinguish between the subgrade and FPL. The boundaries of the numerical model, at the calibration stage, were fixed in all directions to simulate the confined experimentally tested sample.

3.2.1 Modelling parameters

The aim of the 3D modelling was to investigate the deformation of the superstructure under the effect of cyclic loading. Hence, the relevant parameters for this numerical study were the density, Poisson's ratio and Young's modulus. The soil parameters were obtained via DCP and PLT tests and then converted into Young's modulus values. The nature of the cyclic loading was closer to the dynamic behaviour rather than to the static one; therefore dynamic stiffness of rail
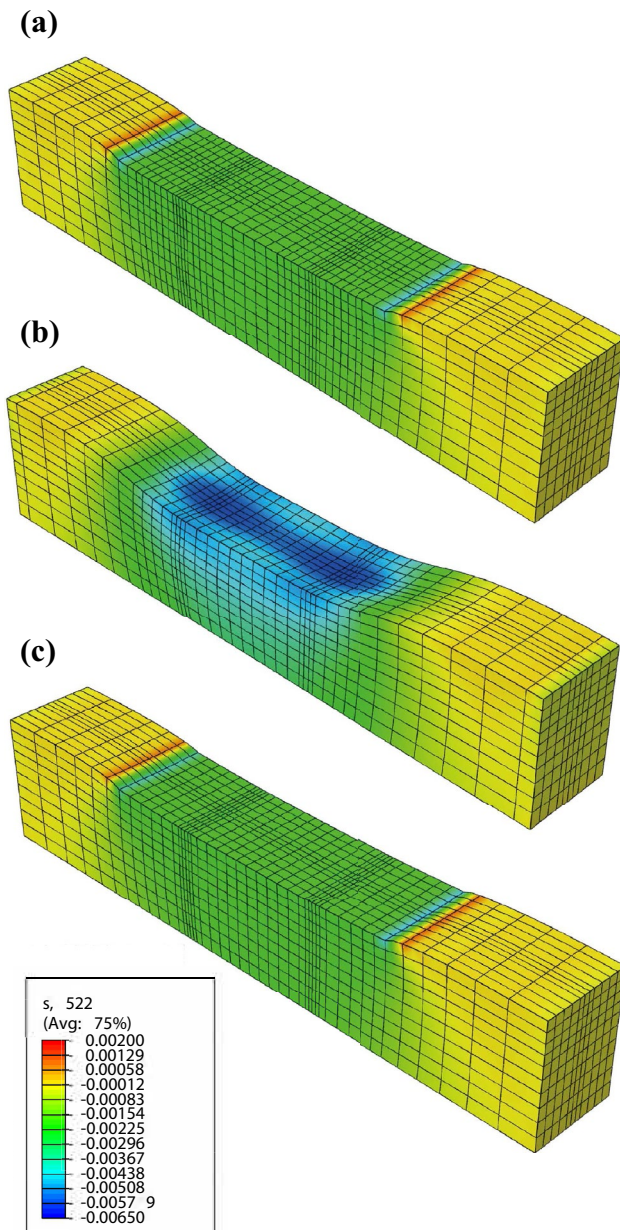
Fig. 10 Stresses in the centre of the soil under the peak of the Cyclic-II: **a** Max-Bögl slab track; **b** ballasted track HBL; **c** NBT slab track
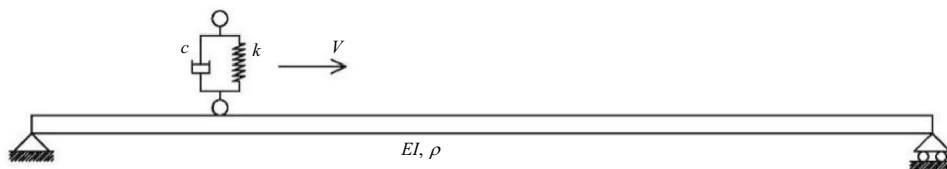
pads, i.e. ethylene vinyl acetate (EVA) and ethylene propylene diene monomer (EPDM) rubber, were considered for the cyclic analysis. The Young's modulus of the pads was calculated based on the stiffness values and dimensions of the pads. Table 1 lists the parameters obtained from the literature and from the pad elements suppliers, which were then compared to the numerical modelling input values. Although the rail segments used in each test had different cross-sectional area, they were made of the same material and. Given their only purpose was to deliver the load from the actuators to the sleepers and the slab in a discrete manner, the same rail profile is used in all 3D models.

3.2.2 Loading and data acquisition

The load applied on each rail in the numerical model was the same as the load applied in the laboratory tests. During the first cyclic test, Cyclic-I, the load applied at 5.6 Hz was oscillating between 13 and 58.9 kN on each rail, giving 117.8 kN per sleeper. Then, during the second cyclic test, Cyclic-II, the load at 2.5 Hz was oscillating between 5 kN and 83.38 kN on each rail, giving 166.76 kN on each sleeper (Fig. 5). To simulate the laboratory testing conditions, the models employed vertical cyclic loading of the test facility, which does not consider the wheel–rail contact.

The amplitude function in Abaqus was employed to deliver the exact experimental load in the numerical models. Two cycles from each tests were used. The duration of the two cycles for Cyclic-I was 0.357 s, standing for 2 cycles occuring in a second at 5.6 Hz loading. The two cycles lasted 0.8 s during Cyclic-II test, for the 2.5 Hz loading. The same durations for the Cyclic-I and Cyclic-II were used for the 3D FEM models. The time increment, i.e. time stepping, was 0.005 s because the sampling rate in in the experimental testing was 200 Hz, meaning that the time difference between two succesive points was 0.005 s. Therefore, the same time increment as the sampling rate during the experiments was used in the models.

The points highlighted in Fig. 6 show the location nodes corresponding to the displacement transducers (LVDT) on the rails and the sleepers in the experimental work. The vertical displacements obtained from the LVDTs were compared against the displacement of these nodes on the models, for which the average of their nodal displacements was considered.
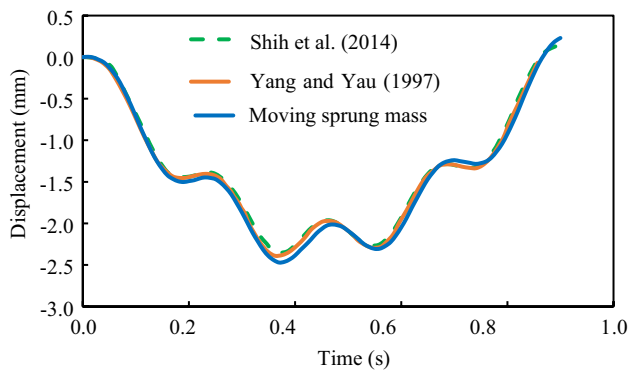

Fig. 11 Motion of the sprung mass on a simply supported beam

Fig. 12 The vertical displacement of the beam

3.2.3 Calibration

The calibration of the slab and ballasted track models were achieved by comparing the numerical and experimental results, for which the vertical displacements were used.

The stresses obtained from the pressure cells were not reliable enough to be used in the calibration process. The high frequency loading prevented the pressure cells to pick up the corrrect stress levels in the soil and, therefore, stress recordings were only used in the experimental study. Figures 7, 8 and 9 show the calibration of the models using rails and sleepers results during the loading. The mechanical properties of the track components and soil were adjusted based on the displacement results. As shown in the figures, the differences are less than 1% indicating very good agreement between the experimental and numerical results. It is worth noting that the experimental results include various errors due to the experimental nature of the work, despite all precautions, which is reflected in the irregular shapes of the curves. Nevertheless, they clearly show the cyclic sinusoidal pattern and they are very close to the numerical results.

The superstructure parameters in the numerical models were taken the same as the values obtained from the experimental work or from the suppliers. However, the soil
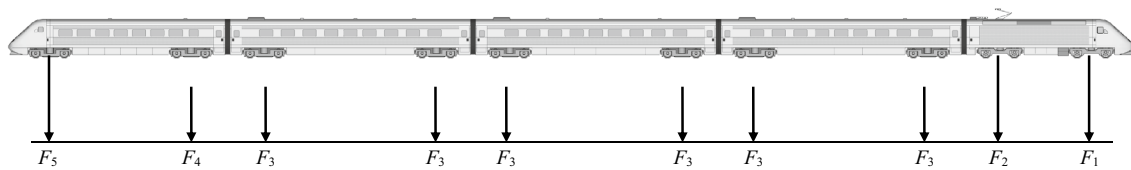

Fig. 13 Real wheel load configuration of the X-2000 train ($F_1 = 181$ kN, $F_2 = 180$ kN, $F_3 = 122$ kN, $F_4 = 117$ kN, and $F_5 = 160$ kN)
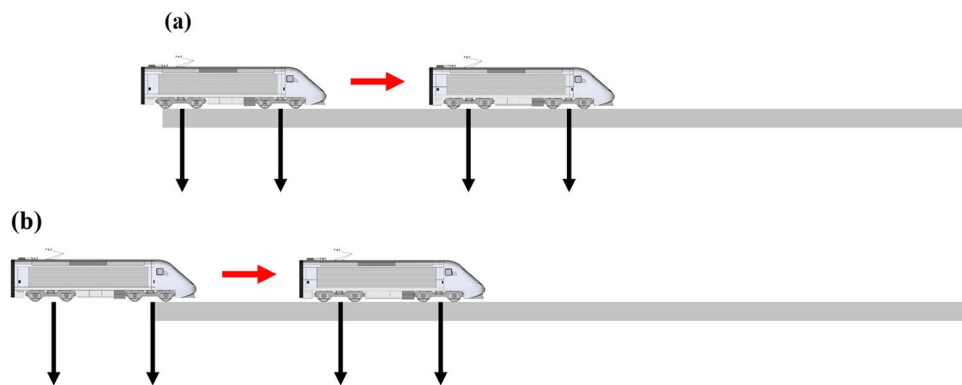

Fig. 14 Train loading scenarios with full axle load at the first time increment: **a** train resting on the track initially; **b** train approaching from outside the domain
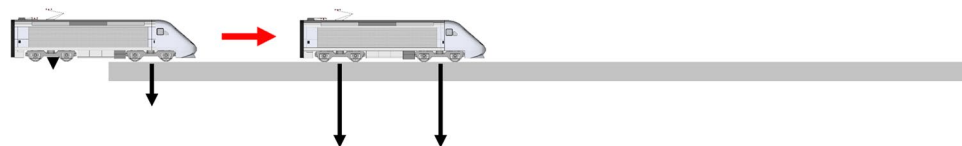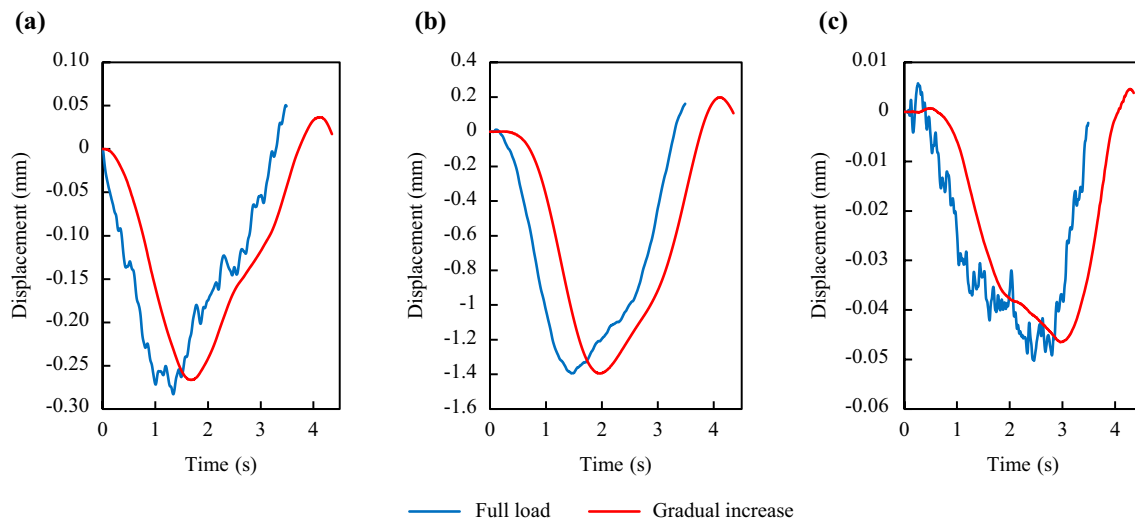

Fig. 15 Train approaching the domain with simultaneous gradual wheel loads increase

Fig. 16 The displacement of the beam at **a** 25 m from the start, **b** 100 m (mid-point) from the start, and **c** 190 m from the start

calibration required more detailed analysis. The elastic properties of the soil were obtained from the *insitu* DCP and PLT tests. The dynamic Young's modulus calculated based on the PLT tests and the equations, proposed by Licthberger [4] and Ramos et al. [61], show significant differences between numerical and experimental input parameters. The values obtained from the in situ tests represent the values during construction of the substructure. These values increased dramatically during testing because of the stiffening of the soil. The DCP tests performed after the experiments proved that the soil stiffness increased three times as shown in Table 2.

After calibrating the slab track parameters with the GRAFT-II experimental results, the NBT slab track was then compared against the Max-Bögl slab track, as illustrated in Fig. 9. These were subjected to Cyclic-I and Cyclic-II loading, as presented previously. The obtained numerical results in terms of displacements at the selected nodal points of the rails and sleepers show that the behaviour of both tracks is very similar. Indeed, the numerical models of the Max-Bögl and NBT slab tracks only show minor differences and, as a consequence, the difference in the obtained results was less than 0.1%.

The numerical results of Figs. 7, 8 and 9 also prove that the elastic displacements of the slab tracks were significantly lower than those of the ballasted track. The displacement of the rail was highly influenced by the railpads. It is estimated that 85% of the rail displacement on the ballasted track was caused by the rail pad and, in the slab track case, it is 95%. Another notable advantage of the slab track was linked to the stress distribution in the soil. As it can be seen from the stress distribution in Fig. 10, the stress levels in FPL were much lower and more uniform than those in the

ballasted track. It is worth noting that the contour plots on the deformed shapes in the figures are made smooth in order to make the contour intervals between the mesh grids continuous. The pressure under the ballast was more focused in the direction of the sleepers, which caused a more concentrated stress area while the slab track distributed the load over a larger area and hence with a reduced stress magnitude. The displacement of the slab was also more uniform unlike in the ballasted track case, where the sleepers displaced more than the ballast located in between the sleepers.

The stress contour plots in the soil, in Fig. 10, show the stress distribution under the tracks and while the stress under the slab track is uniformly distributed over a larger area, the stress distribution was more concentrated locally, i.e. under the sleepers, in the case of ballasted track. The difference between the stress levels under the Max-Bögl track and NBT was negligibly small.

3.3 Train loads

Separate models for the vehicle and the track–ground system can be used to model the dynamic response induced by a moving train. Rigid body models can be used for vehicle components like car bodies, bogies, and wheels. The springs and dampers that link the rigid bodies mimic the primary and secondary suspensions. By defining the nodal forces corresponding to the moving loads as a function of time, the response of a finite element system to the moving loads can be computed. In the case of a moving vehicle, however, the loads are determined by the vehicle's dynamic reaction as well as the track system. To integrate a vehicle multibody model with FE models of the track, a user-defined
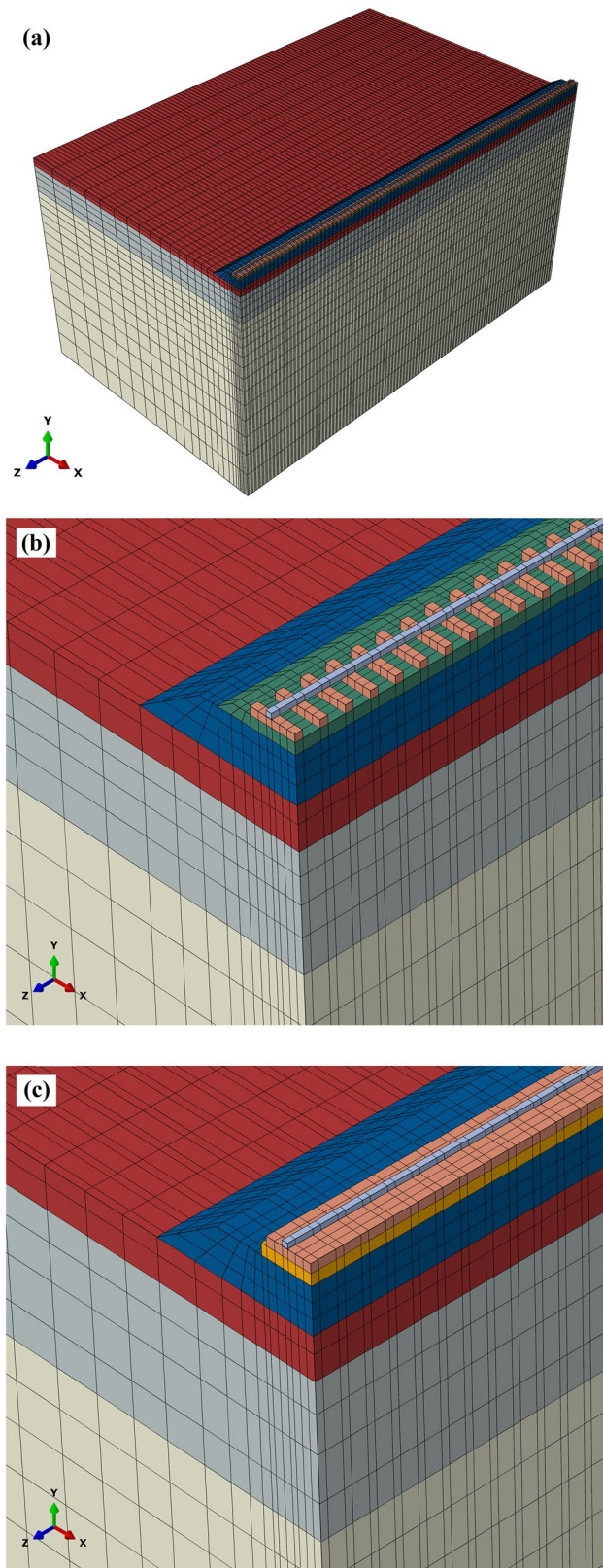
Fig. 17 Three-dimensional track models: **a** track–ground model; **b** close-up view of the ballasted track; **c** close-up view of the NBT

subroutine is usually utilised. Because of the interaction between the two programmes, the simulations take longer times compared to modelling methods without such user-defined subroutines. Instead, an alternative technique has been developed, which makes use of the large (finite) sliding contact model in Abaqus [56]. The technique was validated using the same procedure used by Saleeb and Kumar [55] on a basic moving vehicle–bridge interaction scenario that was simulated without the need of an external subroutine. In summary, this technique entails doing a static analysis, first, followed by an implicit dynamic analysis based on the results of the static analysis. Shih et al. [56] developed this method in Abaqus. The node-to-surface contact feature is used to mimic a sliding motion on a frictionless surface, whereas the default contact attribute "hard contact" is used to simulate the contact dampening. Constant velocity is achieved by specifying the displacement of the moving item along the direction of motion at each time step.

A sprung mass travelling along a simply supported beam, as previously done by Shih et al. [56], was studied in order to clearly present this technique. The motion of the sprung mass on a simply supported beam is illustrated in Fig. 11. The dynamic reaction was compared to the numerical findings produced by Yang and Yau [54] and numerical models by Shih et al. [56]. The following material properties were chosen for the beam: Young's modulus $E = 2.87$ GPa, Poisson's ratio $v = 0.2$, density $\rho = 2303$ kg/m^3, and second moment of area $I = 2.94$ m^4. The values of 1595 kN/m for the suspension stiffness, 0 Ns/m for damping, and 5750 kg for the mass were chosen for the considered configuration. The vehicle speed was taken equal to 27.78 m/s and the bridge length 25 m.

Three dimensional high-order fully integrated quadratic solid elements (C3D20) were utilised to simulate the simply supported beam. The C3D20 elements were used since they are designed to prevent shear locking and hour glassing issues.

The results are in very good agreement with those of Yang and Yau [54] and Shih et al. [56] (Fig. 12). Hence, the sliding contact with sprung mass method was implemented to represent the train loads and the C3D20R elements are used to form the rail in the full dynamic model in this study.

3.4 Load characteristics of the considered train model

As the Ledsgård case was considered in this work for validation purpose, the high-speed passenger train called X-2000 was represented in the models. The train is formed of the locomotive, three passenger carriages and a driving trailer as seen in Fig. 13. Some FE models employed the complete train with all axle loads acting on the track separately [18,
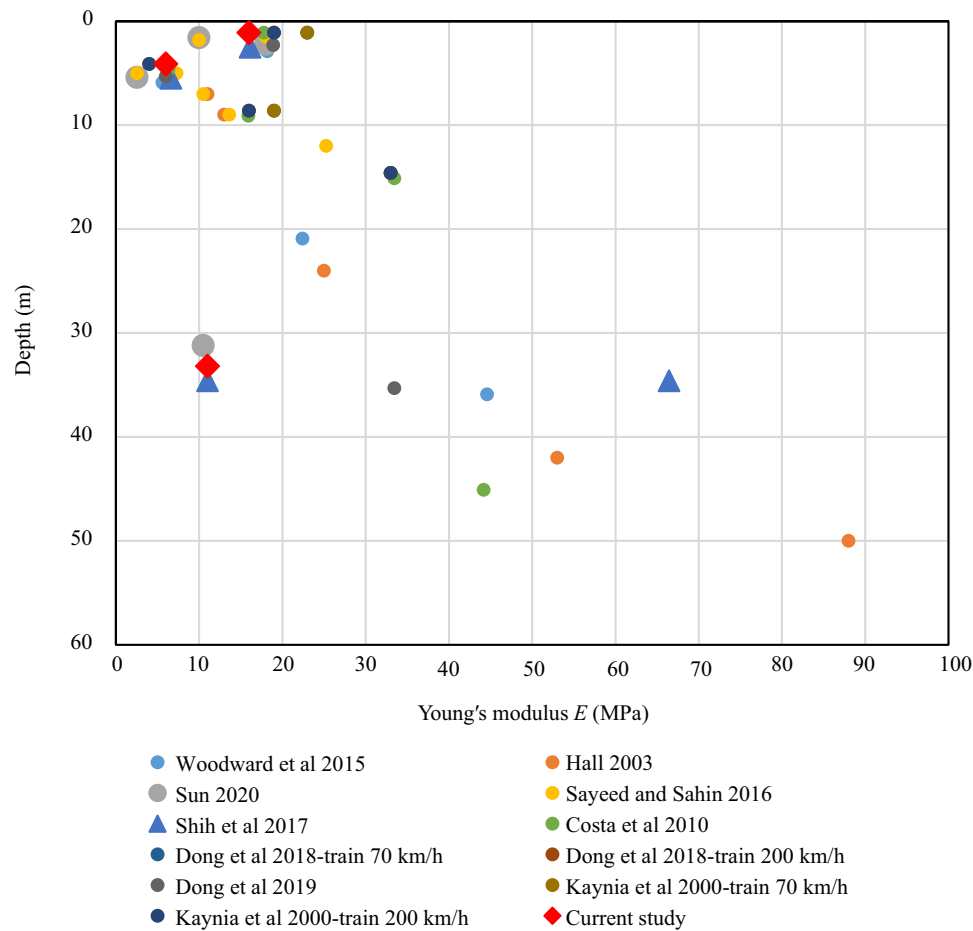
Fig. 18 Soil profile of the Ledsgård field case and numerical models

19, 31], as illustrated in the schematic diagram of Fig. 13, others used bogie loads (combined axles) instead of separate axles [17, 32].

The train modelling in this study follows the same procedure used by Kaynia et al. [17] and Dong et al. [32]. However, to reduce the computational times of the simulations, only first two cars of the train were modelled (Fig. 13), due to largest axle loads present in the locomotive. The locomotive was the heaviest component of the train, so it triggers the highest deflections in the soil, and hence, the peak particle acceleration and velocity were a result of the passage of the locomotive.

One of the major issues of the time-domain train–track dynamic modelling was related to the start of the simulations in which the first loading may lead to an impact effect and hence lead to erroneous results. In this study, various loading scenarios were tested to prevent the initial impact load caused by the first loading. A 200 m long beam is modelled with different moving point load methods. In addition to eliminate the initial impact load effect, the efficiency of

domain size and time step of the model were also taken into account.

One common method is to model the train resting on the track. As soon as the motion of the train starts along with the full axle load at the first time increment (Fig. 14a). The simulation ends with applying full axle load when the train comes to a full stop. This method was found to cause an impact effect by the dynamic load and also not take the advantage of the full domain.

The second method simulates the train in the vicinity of the track. The train approaches the track from outside of the modelled section with full axle load and remains full until the final increment. This method improved the efficiency of the model length. However, full axle load created the impact effect. It was found that to increase the efficiency of the domain, the train must enter the domain from outside, rather than resting on the domain.

In the final method, the train approaches the track from outside the modelled section with no axle load as seen on Fig. 15. Then, all wheel loads are increased gradually up to
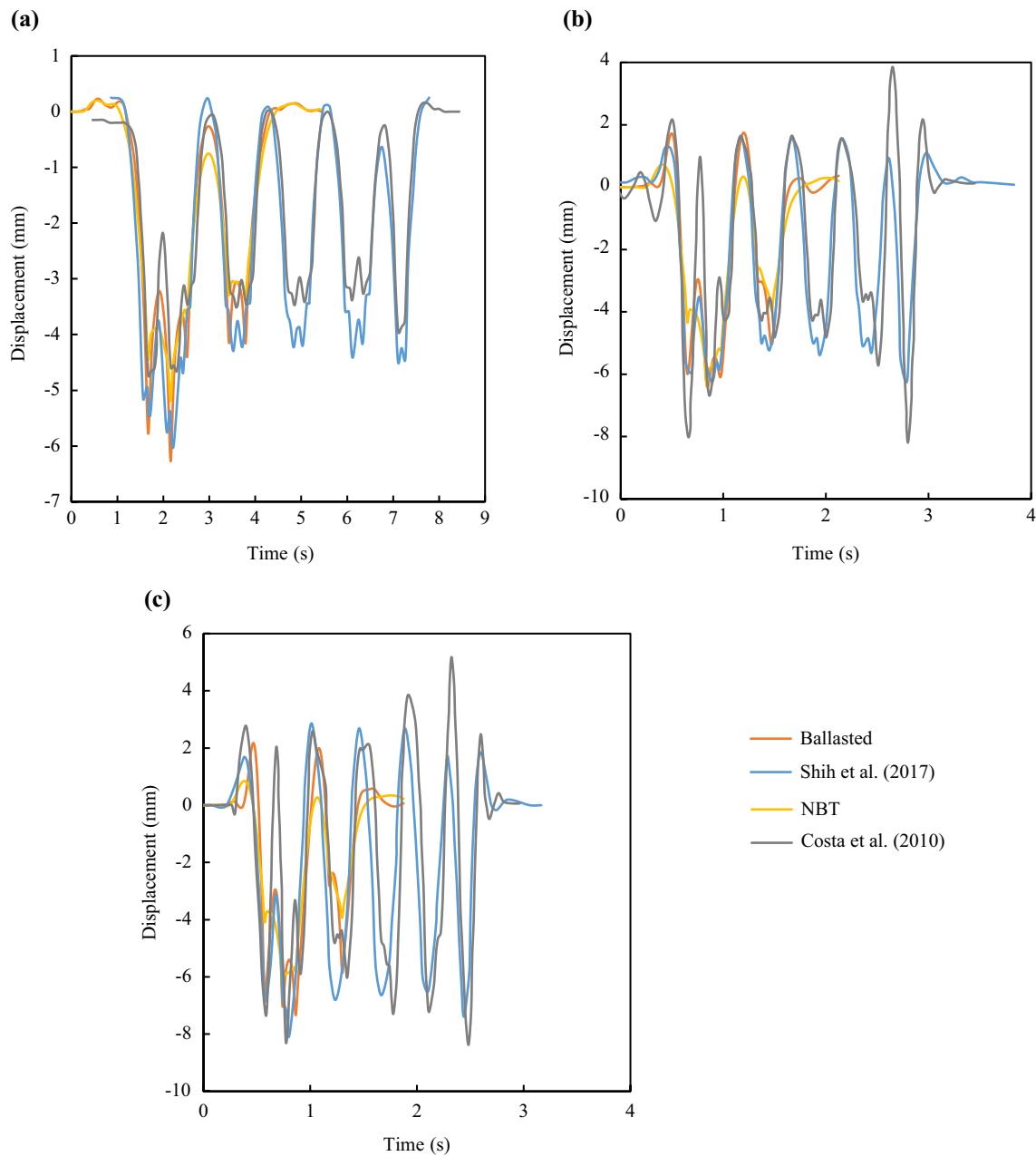
Fig. 19 Displacement of the tracks for the train speeds of **a** 19 m/s, **b** 50 m/s, and **c** 56.67 m/s

the full load, within one time increment, as soon as the first wheels enter the track. When the train leaves the track, at the other end, the wheel loads are gradually reduced, within one time increment. This method was found to prevent the impact effect and the vibrations of the rail beam, and it allowed to simulate the train passage on the full length of the model. This train load increasing within a time can reduce further fluctuations as it can mimic an initial static loading on the track.

Figure 16 illustrates the displacements of the nodes of the beam under all loading methods at 25 m, 100 m (midpoint) and 190 m, respectively. As it can be seen, when the full axle load was applied at the first increment, it caused impact effect and vibrations in the beam. However, gradual increase method was chosen for the dynamic model analysis, in this study, because it resolved the impact load effect as well as the vibration issues in the beam without employing the two-step solution, which consists of the
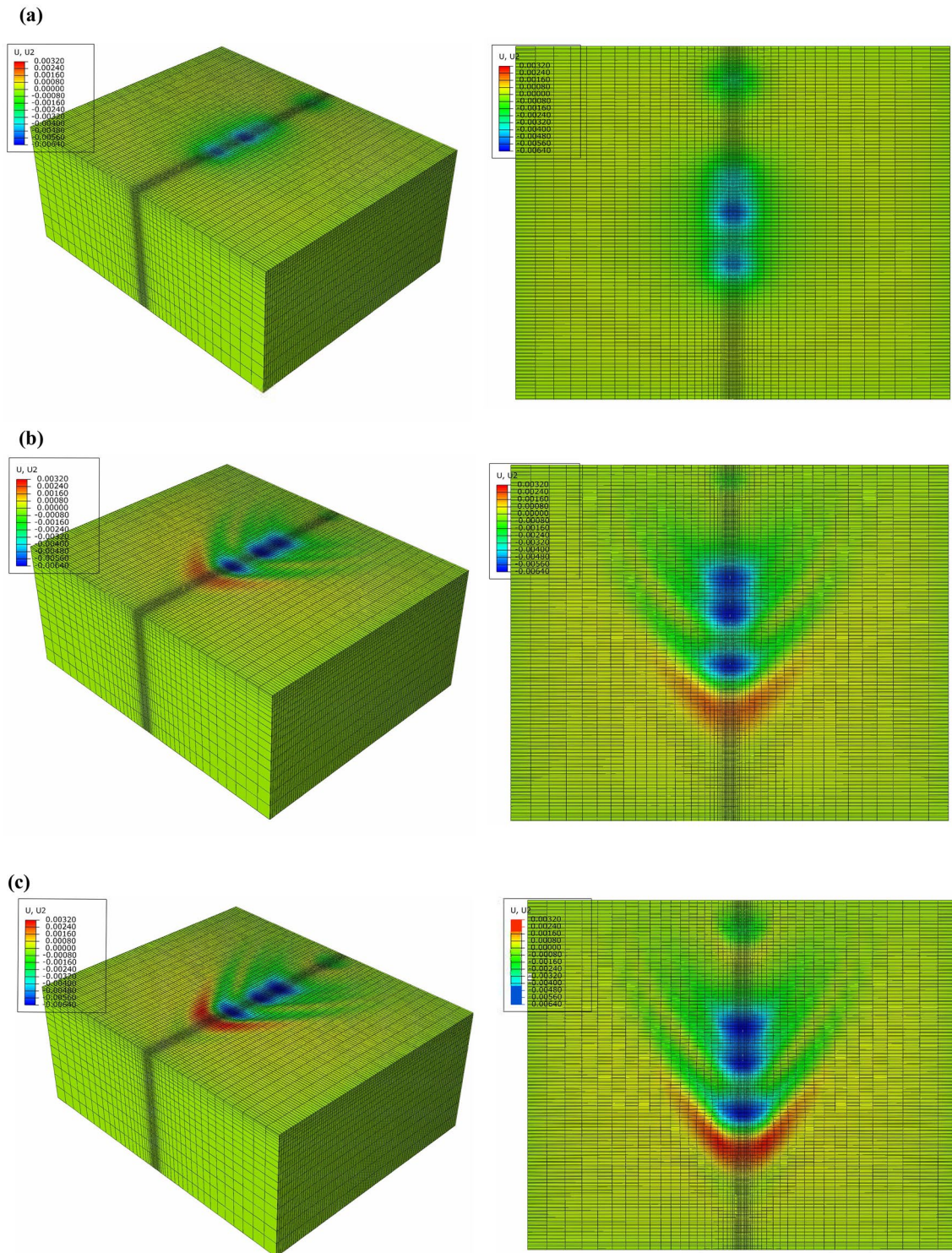
Fig. 20 Contour plots of ground waves of the ballasted track at **a** 19 m/s, **b** 50 m/s, and **c** 56.67 m/s (the superstructure was removed for clarity)

initial static loading step followed by the dynamic loading step. This reduced the required simulation time and allows to simulate the train passage on the full length of the track.

The figures also indicate a sudden displacement for full axle load methods which does not represent a realistic train approach as the displacement should develop in a
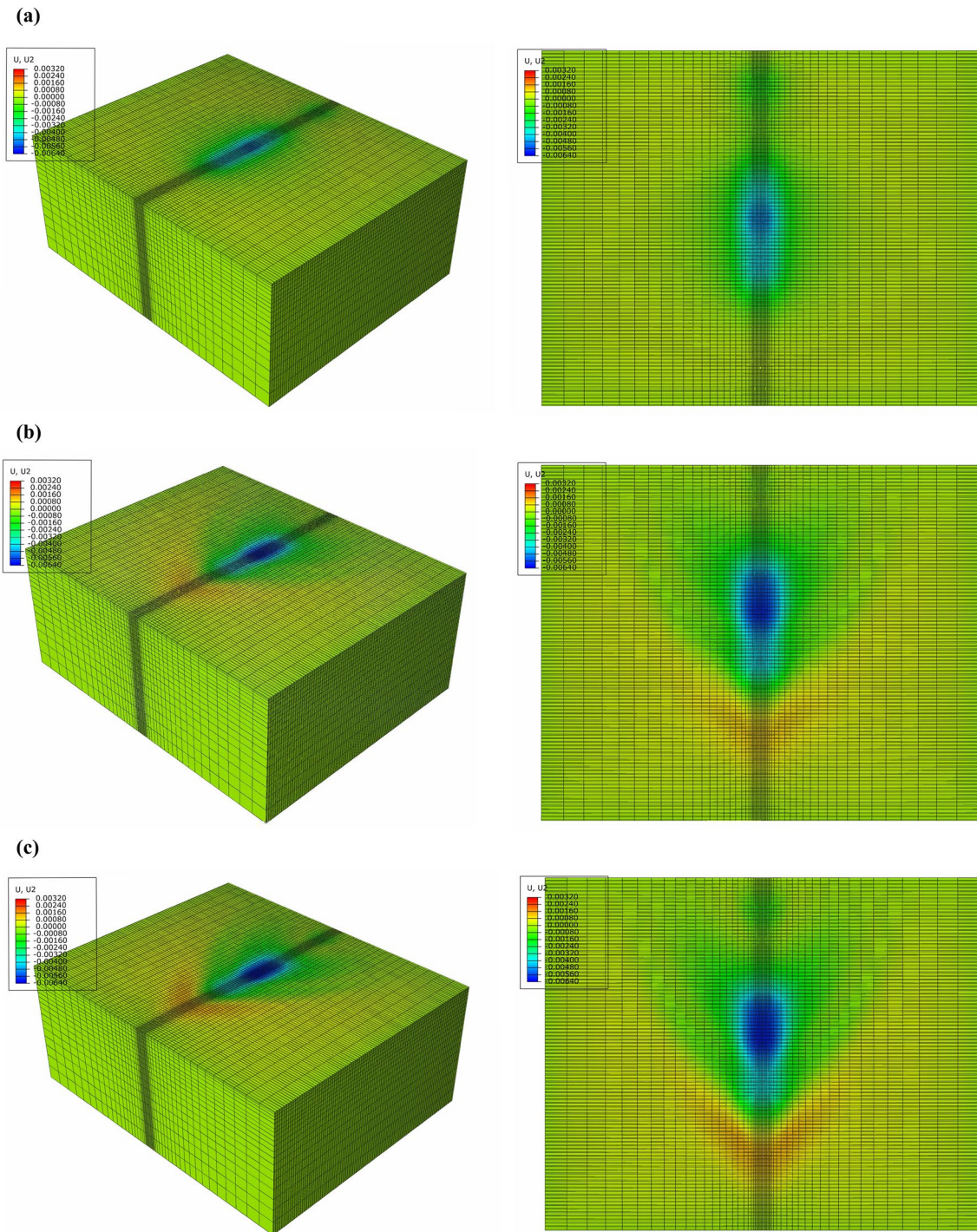
Fig. 21 Contour plots of ground waves of the NBT at **a** 19 m/s, **b** 50 m/s, and **c** 56.67 m/s (the superstructure was removed for clarity)

gradual trend, as seen in gradual increase method. Additionally, the fluctuations in the lines disappeared when the approaching trains with gradual load increase model is employed.

3.5 Full dynamic model

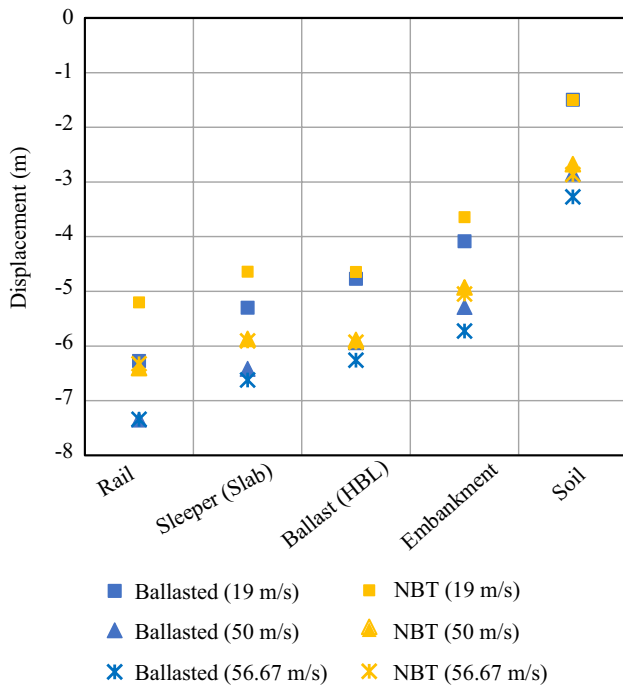A three-dimensional finite element model was created in Abaqus for the dynamic analysis of the considered

Fig. 22 Maximum displacements of the components of the ballasted track and NBT at various speeds
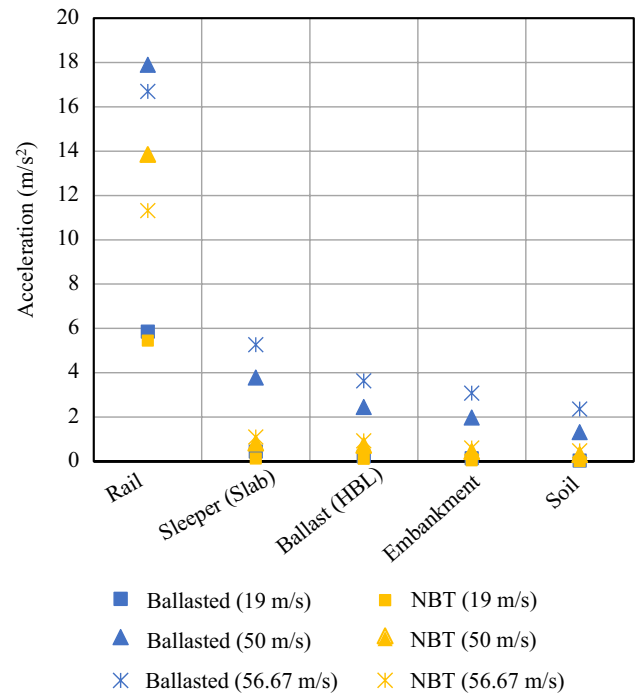

Fig. 24 Peak particle acceleration (PPA) of the components of the ballasted track and NBT at various speeds
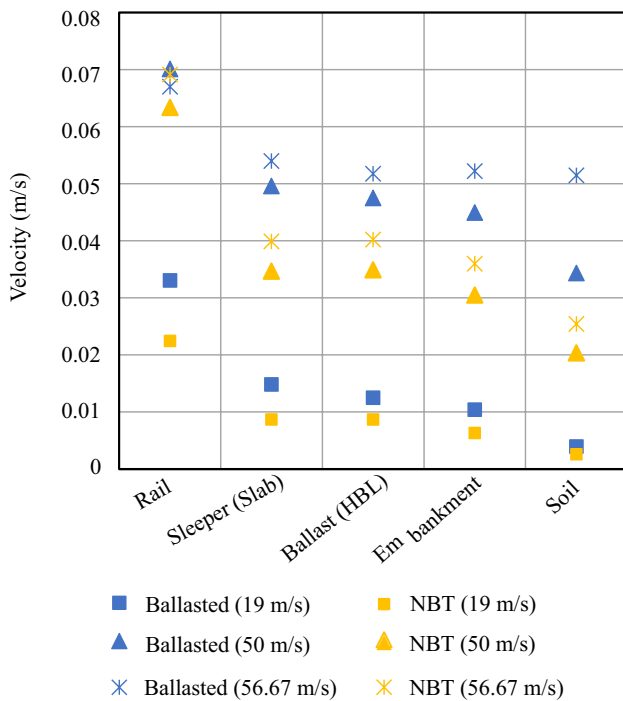

Fig. 23 Peak particle velocity (PPV) of the components of the ballasted track and NBT at various speeds

train–track–soil problem, as shown in Fig. 17a. The model consisted of 110,700 elements and 125,218 nodes. The track and soil mesh grids were made of 8-node C3D8R cubic elements, and the UIC60 rail was represented by rectangular beam C3D20R quadratic elements. The second moment of area of the beam was chosen the same as the UIC60 rail second moment of area. The element sizes of the soil were gradually increased away from the track in the horizontal and vertical directions. The soil domain was 65 m long, 40 m wide and 33.3 m deep. The FE model was relatively large, but the symmetry of the problem allows us to only consider half of the model. Indeed, the axis along the rails passing through the mid points of the sleepers defined two halves of the model, which would behave in the same manner given the symmetry of the geometry and loading conditions. As a result, the model was reduced to 55,350 elements and 62,609 nodes, leading to a significant reduction of the computational effort and CPU time.

The nodes at the bottom and lateral side boundaries of the models were fixed to prevent any translation or rotation movement. As the deflections of the centre of the track were recorded, the non-reflecting boundary conditions were not employed in the model. It was reported by Shih et al. [64] that the absorbing boundary conditions were not required if the model was large enough. This was because the incorporated damping model with a sufficiently enough mass-proportional term allows for energy dissipation and

eliminates the possibility of wave reflections at the boundaries. Therefore, this study used a Rayleigh damping model with a damping ratio of 4%, as indicated by Hall [19]. Another reason for not using infinite elements as boundary conditions was to take advantage of the parallelization function of Abaqus. Given the above data, the time increment is specified as 10^{-3} s in the Refs. [19, 65], with the minimum increment being 10^{-4} s.

The Ledsgård case study was used here to validate the developed models. The Young's modulus values of the soil layers are indicated in Fig. 18. The rail pads with the stiffness of 4.7×10^8 N/m were used to connect the rail to the sleepers or to the slab, in the slab track case.

4 Numerical analysis

The Ledsgård field data for train speeds of 19, 50 and 56.67 m/s were publicly available and hence were used in the validation process of the developed models in this study. The time history of the vertical track deflections for the train speed of 70 km/h (19 m/s) are shown in Fig. 19. The simulation results of the linear models of Costa et al. [31] and Shih et al. [65] were used in this validation. This speed was lower than the ground's lowest shear wave velocity, indicating a subseismic state. As a result, the displacement field had a quasi-static character. Since the model was linear, the soil stiffness parameters remained constant for all train speeds, unlike the nonlinear soil models which employed lower stiffness values and higher damping ratios for higher train speeds [17, 33, 65]. Figure 19b andc shows the vertical displacements of the track for a train travelling at 180 km/h (50 m/s) and 204 km/h (56.67 m/s), respectively. Both tain speeds were close to the critical velocity of the track. As shown in the figures, overall, there was good agreement between the NBT and ballasted track models, and the available results from the literature for the considered linear models. It is worth noting that the results shown in Fig. 19 exhibit some differences. These were due to the different modelling appoaches used or differences in modelling details, which may not be indicated in the literature. This may also be due to differences in the analysis parameters, such as mesh size or time increment. However, the displacements from all models indicated similar values and similar behaviour.

The contour plots in Figs. 20 and 21 illustrate the development of the Mach cone and the resonant train–track state. The Mach cone started forming when the train speed approached the subgrade Rayleigh wave velocity. In Figs. 20b and 21b, the cone is clearly visible. The Mach cone was seen and easily distinguishable due to track deflection. Damping would have a big influence on the final pattern.

Several studies have been published on the ballast peak particle velocity (PPV) and peak particle acceleration (PPA) thresholds to cause ballast movement. According to Pita et al. [66], PPV levels above 15–18 mm/s result in ballast deterioration and loss of compaction. According to Baeβler et al. [67], if ballast accelerations exceed 0.7–0.8 g, where g is the gravity acceleration, the ballast will begin to decompact and a limit of $0.35g$ was established as a result. Banimahd et al. [68] showed through numerical results the change of PPV with speed, including critical velocity cases, with identifying areas of low, medium, and high maintenance. Having relatively high PPV or PPA values makes ballast fly, potentially coupled with severe wind shear from passing trains. The peak deflections, PPV and PPA of the ballasted track and NBT nodal points are plotted in Figs. 22, 23 and 24, respectively. The ballast acceleration at low speeds was $0.22g$, and the node at the HBL shows $0.11g$ which were both within the limits stated by Baeβler et al. [67]. However, near the critical velocity, the ballast acceleration increased to $3.63g$ and the HBL to $0.7g$. The PPV values of the ballast increased from 12 to 47 mm/s when the train speed reached the critical velocity. The PPV values of the HBL in the NBT was around 30% less than that of the ballasted track.

5 Conclusion

In this paper, three-dimensional finite element modelling was carried out in Abaqus to investigate the performance of the new ballastless track (NBT) for high-speed railways and compare its performance to that of a ballasted track. The developed models were calibrated using outputs of full-scale laboratory testing carried out in GRAFT facility at Heriot Watt University.

First, models representing the ballasted and slab track sections tested in GRAFT II facility were developed in Abaqus and calibrated using the experimental results. Then, the NBT model was developed and compared against the calibrated slab track results. Both NBT and ballasted track models were finally extended to deal with the track geodynamics due to the passage of a train represented by multiple moving point loads. Different train loading methods were presented and the most practical method was used in the investigation of train speed effects, including the critical track velocity effect.

On top of the adopted modelling approach in this work, a correlation expression between the dynamic cone penetrometer (DCP) readings and California bearing ratio (CBR) values was proposed and the deflection modulus E_{V2} was verified using a static plate load test. The main conclusions are obtained as follows:

1. Due to the presence of the hydraulically bonded rigid layer and the reinforced concrete layer, the slab tracks deflect significantly less than the sleepers present in the

ballasted tracks. The stress levels are distributed over a larger area under the slab tracks, while the stress distribution is focused beneath the sleepers in the ballasted tracks.

2. The Young's modulus used in the numerical models are based on the correlations of CBR and E_{V2} values. The Young's modulus is found to be 4 times E_{V2} values collected by the plate load tests and 10 times the CBR values obtained with the dynamic cone penetrometer tests.

3. The finite sliding contact model with a moving oscillator is used to simulate the dynamic train loading allowing the train to pass through the entire length of the model. This loading method allows the train to approach the track from outside of the modelled computational domain. This efficient loading method allows for gradual deflection development in the tracks and eliminates the impact effect as well as the displacement fluctuations in the rail.

4. When trains traverse at speeds close to the critical track velocity, large track displacements are exhibited. Under all considered train speeds, the NBT slab track deflected less than the ballasted track in all considered train speed cases. At speeds close to the critical velocity, Mach cones begin to form.

5. One of the notable effects is the uplift motion of the NBT, which was substantially smaller than that of the ballasted track. At critical speeds, in particular, the ballasted track exhibits significant track uplift. The maximum uplift and downward vertical displacement occurred in the ballasted track under the train load running at 57 m/s. The contour plots reveal that the NBT caused lower downward and upward displacements in the soil

6. The peak particle acceleration values of the sleeper, embankment and soil are about 5 times higher in the ballasted track than in the slab track, and the peak particle velocity values in the ballasted track are 1.5 times higher than in the slab track.

The above conclusions are of primary importance for practitioners in railway infrastructure. The developed modelling of NBT and ballasted tracks could be further enhanced by considering other parameters which may significantly influence their performances, such as material or geometric nonlinearities.

References

1. El Kacimi A, Woodward PK, Laghrouche O, Medero G (2013) Time domain 3D finite element modelling of train-induced vibration at high speed. Comput Struct 118:66–73
2. Esveld C (2001) Modern railway track. MRT-productions, Zaltbommel
3. Darr E (2000) Ballastless track: design, types, track stability, maintenance and system comparison. Railw Tech Rev 3:36–45
4. Lichtberger B (2005) Track compendium. Eurailpress, Hamburg, pp 1–192
5. Bastin R (2006) Development of German non-ballasted track forms. Proc Inst Civ Eng Transp 159(1):25–39
6. Kiani M, Parry T, Ceney H (2008) Environmental life-cycle assessment of railway track beds. Proc Inst Civ Eng Eng Sustain 161(2):135–142
7. Gautier PE (2015) Slab track: review of existing systems and optimization potentials including very high speed. Constr Build Mater 92:9–15
8. Robertson I, Masson C, Sedran T, Barresi F, Caillau J, Keseljevic C, Vanzenberg JM (2015) Advantages of a new ballastless trackform. Constr Build Mater 92:16–22
9. Esveld C (2003) Recent developments in slab track. Eur Railw Rev 9(2):81–85
10. Esveld C (1997) Innovations in railway track. TU Delft, Delft, pp 1–12
11. Marolt Čebašek T, Esen AF, Woodward PK, Laghrouche O, Connolly DP (2018) Full scale laboratory testing of ballast and concrete slab tracks under phased cyclic loading. Transp Geotech 17:33–40
12. Esen AF, Woodward PK, Laghrouche O, Connolly DP (2022) Stress distribution in reinforced railway structures. Transp Geotech 32:100699
13. Connolly D (2013) Ground borne vibrations from high speed trains. Heriot-Watt University, Edinburgh
14. Woodward PK, Laghrouche O, Mezher SB, Connolly DP (2015) Application of coupled train–track modelling of critical speeds for high-speed trains using three-dimensional non-linear finite elements. Int J Railw Tech 4(3):1–35
15. Mezher SB, Connolly DP, Woodward PK, Laghrouche O, Pombo J, Costa PA (2016) Railway critical velocity–analytical prediction and analysis. Transp Geotech 6:84–96
16. Madshus C, Kaynia AM (2000) High-speed railway lines on soft ground: dynamic behaviour at critical train speed. J Sound Vib 231(3):689–701
17. Kaynia AM, Madshus C, Zackrisson P (2000) Ground vibration from high-speed trains: prediction and countermeasure. J Geotech Geoenviron Eng 126(6):531–537

18. Takemiya H (2003) Simulation of track–ground vibrations due to a high-speed train: the case of X-2000 at Ledsgard. J Sound Vib 261(3):503–526

19. Hall L (2003) Simulations and analyses of train-induced ground vibrations in finite element models. Soil Dyn Earthq Eng 23(5):403–413

20. Gao Y (2016) Field and analytical investigation of a 3D dynamic train–track interaction model at critical speeds. Pennsylvania State University, State College

21. Atalan M, Prendergast LJ, Grizi A, Thom N (2022) A review of numerical models for slab-asphalt track railways. Infrastructures 7(4):59

22. Timoshenko SP (1926) Methods of analysis of statical and dynamical stresses in rail. In: Proceeding of the second international congress for applied mechanics, Zurich, Switzerland, 1926, pp 407−418

23. Kalker JJ (1996) Discretely supported rails subjected to transient loads. Veh Syst Dyn 25(1):71–88

24. Nsabimana E, Jung YH (2015) Dynamic subsoil responses of a stiff concrete slab track subjected to various train speeds: a critical velocity perspective. Comput Geotech 69:7–21

25. Andersen L, Jones CJC (2006) Coupled boundary and finite element analysis of vibration from railway tunnels—a comparison of two- and three-dimensional models. J Sound Vib 293(3–5):611–625

26. Bian XC, Chen YM, Hu T (2008) Numerical simulation of high-speed train induced ground vibrations using 2.5D finite element approach. Sci China Ser G 51(6):632–650

27. Lombaert G, Degrande G, Kogut J, François S (2006) The experimental validation of a numerical model for the prediction of railway induced vibrations. J Sound Vib 297(3–5):512–535

28. François S, Galvín P, Schevenels M, Lombaert G, Degrande GA (2012) 25D coupled FE–BE methodology for the prediction of railway induced vibrations. In: Schulte-Werning B, Thompson D, Gautier PE, Hanson C, Hemsworth B, Nelson J, Maeda T, de Vos P (eds) Noise and Vibration mitigation for rail transportation systems. Springer, Tokyo, pp 367–374

29. Costa PA, Colaço A, Calçada R, Cardoso AS (2015) Critical speed of railway tracks. Detailed simplified approaches. Transp Geotech 2:30–46

30. Connolly DP, Galvín P, Olivier B, Romero A, Kouroussis G (2019) A 2.5D time-frequency domain model for railway induced soil-building vibration due to railway defects. Soil Dyn Earthq Eng 120:332–344

31. Alves Costa P, Calçada R, Silva Cardoso A, Bodare A (2010) Influence of soil non-linearity on the dynamic response of high-speed railway tracks. Soil Dyn Earthq Eng 30(4):221–235

32. Dong K, Connolly DP, Laghrouche O, Woodward PK, Alves Costa P (2019) Non-linear soil behaviour on high speed rail lines. Comput Geotech 112:302–318

33. Dong K, Connolly DP, Laghrouche O, Woodward PK, Alves Costa P (2018) The stiffening of soft soils on railway lines. Transp Geotech 17:178–191

34. Galvín P, Romero A, Domínguez J (2010) Fully three-dimensional analysis of high-speed train–track–soil–structure dynamic interaction. J Sound Vib 329(24):5147–5163

35. Banimahd M, Woodward PK, Kennedy J, Medero GM (2012) Behaviour of train–track interaction in stiffness transitions. Proc Inst Civ Eng Transp 165(3):205–214

36. Shih JY, Thompson DJ, Zervos A (2017) The influence of soil nonlinear properties on the track/ground vibration induced by trains running on soft ground. Transp Geotech 11:1–16

37. Sun QD, Indraratna B, Grant J (2020) Numerical simulation of the dynamic response of ballasted track overlying a tire-reinforced capping layer. Front Built Environ 6:1–15

38. Abu Sayeed M, Shahin MA (2016) Three-dimensional numerical modelling of ballasted railway track foundations for high-speed trains with special reference to critical speed. Transp Geotech 6:55–65

39. Lysmer J, Kuhlemeyer RL (1971) Closure to "finite dynamic model for infinite media." J Engrg Mech Div 97(1):129–131

40. Connolly D, Giannopoulos A, Forde MC (2013) Numerical modelling of ground borne vibrations from high speed rail lines on embankments. Soil Dyn Earthq Eng 46:13–19

41. Connolly D, Giannopoulos A, Fan W, Woodward PK, Forde MC (2013) Optimising low acoustic impedance back-fill material wave barrier dimensions to shield structures from ground borne high speed rail vibrations. Constr Build Mater 44:557–564

42. Gao Y, Huang H, Ho CL, Judge A (2018) Field validation of a three-dimensional dynamic track–subgrade interaction model. Proc Inst Mech Eng Part F J Rail Rapid Transit 232(1):130–143

43. Gao Y, Huang H, Ho CL, Hyslip JP (2017) High speed railway track dynamic behavior near critical speed. Soil Dyn Earthq Eng 101:285–294

44. Theyssen JS, Aggestam E, Zhu S, Nielsen JCO, Pieringer A, Kropp W, Zhai W (2021) Calibration and validation of the dynamic response of two slab track models using data from a full-scale test rig. Eng Struct 234:111980

45. Zhai W, Wang K, Chen Z, Zhu S, Cai C, Liu G (2020) Full-scale multi-functional test platform for investigating mechanical performance of track–subgrade systems of high-speed railways. Railw Eng Sci 28(3):213–231

46. Luo J, Zhu S, Zhai W (2021) An advanced train–slab track spatially coupled dynamics model: theoretical methodologies and numerical applications. J Sound Vib 501:116059

47. Zhu S, Cai C (2014) Interface damage and its effect on vibrations of slab track under temperature and vehicle dynamic loads. Int J Non Linear Mech 58:222–232

48. Yang J, Zhu S, Zhai W, Kouroussis G, Wang Y, Wang K, Lan K, Xu F (2019) Prediction and mitigation of train-induced vibrations of large-scale building constructed on subway tunnel. Sci Total Environ 668:485–499

49. Qu S, Zhao L, Yang J, Wu Z, Zhu SY, Zhai W (2023) Numerical analysis of engineered metabarrier effect on ground vibration induced by underground high-speed train. Soil Dyn Earthq Eng 164:107580

50. Frýba L (1972) Moving random loads. In: Frýba L (ed) Vibration of solids and structures under moving loads. Springer, Dordrecht, pp 410–427

51. Krylov VV (1995) Generation of ground vibrations by superfast trains. Appl Acoust 44(2):149–164

52. Dieterman H, Metrikine A (1996) The equivalent stiffness of a half-space interacting with a beam. Critical velocities of a moving load along the beam. Euro J Mech Ser Solids 15:67–90

53. Kouroussis G, Verlinden O, Conti C (2009) Ground propagation of vibrations from railway vehicles using a finite/infinite-element model of the soil. Proc Inst Mech Eng Part F J Rail Rapid Transit 223(4):405–413

54. Yang YB, Yau JD (1997) Vehicle–bridge interaction element for dynamic analysis. J Struct Eng 123(11):1512–1518

55. Saleeb AF, Kumar A (2011) Automated finite element analysis of complex dynamics of primary system traversed by oscillatory subsystem. Int J Comput Meth Eng Sci Mech 12(4):184–202

56. Shih JY, Thompson D, Zervos A (2014) Assessment of track–ground coupled vibration induced by high-speed trains. In: The 21st international congress on sound and vibration, 13–17 July, 2014, Beijing

57. Esen AF, Woodward PK, Laghrouche O, Čebašek TM, Brennan AJ, Robinson S, Connolly DP (2021) Full-scale laboratory testing of a geosynthetically reinforced soil railway structure. Transp Geotech 28:100526

58. BSI (1990) B. 1377–4–1990, "BS 1377–4–1990, methods of test for Soils for civil engineering purposes-Part4: compaction-related tests,." British Standard institute, London

59. TRRL (1990) Overseas road note 8: a users manual for a program to analyse dynamic cone penetrometer data. Transport and Road Research Laboratory, Crowthorne, Berkshire

60. DIN (2001) DIN18134, Determining the deformation and strength characteristics of soil by the plate loading test, 2001.

61. Ramos A, Gomes Correia A, Calçada R, Alves Costa P, Esen A, Woodward PK, Connolly DP, Laghrouche O (2021) Influence of track foundation on the performance of ballast and concrete slab tracks under cyclic loading: physical modelling and numerical model calibration. Constr Build Mater 277:122245

62. Sainz-Aja JA, Carrascal IA, Ferreño D, Pombo J, Casado JA, Diego S (2020) Influence of the operational conditions on static and dynamic stiffness of rail pads. Mech Mater 148:103505

63. Thölken D, Abdalla Filho JE, Pombo J, Sainz-Aja J, Carrascal I, Polanco J, Esen A, Laghrouche O, Woodward P (2021) Three-dimensional modelling of slab–track systems based on dynamic experimental tests. Transp Geotech 31:100663

64. Shih JY, Thompson DJ, Zervos A (2016) The effect of boundary conditions, model size and damping models in the finite element modelling of a moving load on a track/ground system. Soil Dyn Earthq Eng 89:12–27

65. Shih JY, Thompson DJ, Zervos A (2018) Modelling of ground-borne vibration when the train speed approaches the critical speed. In: Schulte-Werning B, Thompson D, Gautier PE, Hanson C, Hemsworth B, Nelson J, Maeda T, de Vos P (eds) Noise and vibration mitigation for rail transportation systems. Springer, Cham, pp 497–508

66. Lopez Pita A, Teixeira PF, Robuste F (2004) High speed and track deterioration: the role of vertical stiffness of the track. Proc Inst Mech Eng Part F J Rail Rapid Transit 218(1):31–40

67. Baeßler M, Bronsert J, Cuéllar P, Rücker W (2012) The stability of ballasted tracks supported on vibrating bridge decks, abutments and transition zones. In: Proceedings of the first international conference on railway technology: research, development and maintenance, vol 13. Civil-Comp Press, Stirlingshire

68. Banimahd M, Woodward P, Kennedy J, Medero G (2013) Three-dimensional modelling of high speed ballasted railway tracks. Proc Inst Civ Eng Transp 166(2):113–123